Continuous-Flow Synthesis of Aspirin on a Microfluidic Device with Chaotic Mixer

Abstract

Continuous-flow synthesis of compounds has been of increasing interest in the last decennium as it gives room to automatization and optimisation. In this study a microfluidic system with passive staggered herringbone mixer was developed to investigate continuous-flow aspirin production. Optimal conditions for aspirin synthesis were analysed in this system. The efficiency of this new system was compared to the batch synthesis based on yield, purity and salicylic acid content. Production of aspirin in the microfluidic system was successful. The continuous flow system had a yield of 78%, purity of 92% and an salicylic content of 2.4%. For the batch process this was 81%, 97% and a negligible amount. The yields of both processes were similar, with the batch synthesis having a higher purity.

Name: Mirjam Brinkman

S-number: S3920240

Date: 7 February 2022 – 8 April 2022

Supervisor: Dr Pim de Haan

Research Group: Pharmaceutical Analysis

Inhoud

1. Introduction

Microfluidics: Turbulent vs Laminar Flow

The chemical and physical characteristics in behaviour of fluids and gases are different in a microenvironment compared to on a larger scale. The flow properties of liquids play a very important role in the microsystems. At the meter scale, liquids have a turbulent flow characterised by irregular and chaotic movements of the fluid streams (figure 1) (1). This allows for spontaneous and lateral mixing. At the microscale, parameters such as viscosity and surface tension play a more important role as well as diffusion (2). The fluid streams in such a system move in smooth paths called laminar flow. The parameter that predicts how liquids will behave in a system is the Reynolds number. The Reynolds number is a unitless parameter that represents the ratio between the inertial forces and the viscous forces in a system. Turbulent flow occurs in systems with a high Reynolds number (> 4000) and laminar flow in systems with a low Reynolds number (<2000) (3). There are two equations to calculate this parameter, which are shown in figure 2 with the L being the characteristic length of the channels which is presented as the diameter.

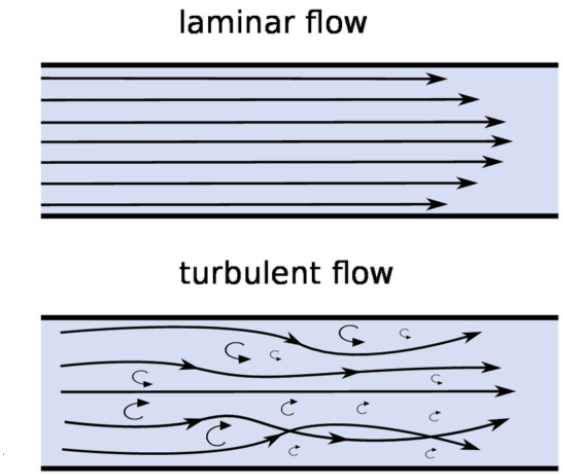

Figure 1: Visual representation of fluid stream movement in laminar and turbulent flow (4).

$$Re = \frac{\rho \cdot V \cdot L}{\mu} \; or \; Re = \frac{V \cdot L}{\nu}$$

Figure 2: Two equations for calculating the Reynolds number. Adapted from (5). *ρ = density (g/cm^3); V = velocity (m/s); L = length (m); μ = Bulk viscosity (Pa*s); ν = kinematic viscosity (m^2/s). Re = Reynolds number (unitless)*

In laminar flow, no mixing between fluid streams occurs by eddies as in turbulent flow, only diffusion works at the interface of the liquid streams (6). Diffusion is a passive and slow mechanism, so to efficiently mix two or more fluid streams in microsystems, a mixer needs to implemented. Mixing is an essential step in chemical and pharmaceutical synthesis.

Mixers: Active vs Passive

There are two main categories of mixers: active and passive. The mechanism behind active mixers is the application of an external force to achieve mixing in the microsystem. A broadly used method is acoustic or supersonic mixing where an acoustic field is created in a fluid disrupting the laminar flow also called acoustic streaming (7,8). Another mixing technique is thermal mixing where by heating the fluid streams on one side they are encouraged to mix (9). Other options are mixing by pressure differences by adding peristaltic pumps (10) and magnetically with rotating fields (11).

Contrary to active mixers, passive mixers do not use external force but instead optimize the channel shape and geometry to achieve an optimal interface between the liquid streams (7). Passive mixers have as advantage that they are generally easier to implement in the microsystem.

One of the most simple and straightforward passive mixers is the planar squarewave mixer shown in figure 3 (12). It uses 90° angles to shift liquid streams out of their original path and causes secondary flow-back due to the centrifugal force (13). These two things lead to increased mixing. Figure 4 shows the three dimensional serpentine mixer, which is the more efficient version of the squarewave mixer (12).

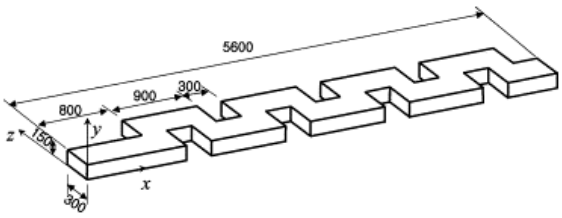

Figure 4: A planar squarewave mixer with a sequence of 90° turns (12).

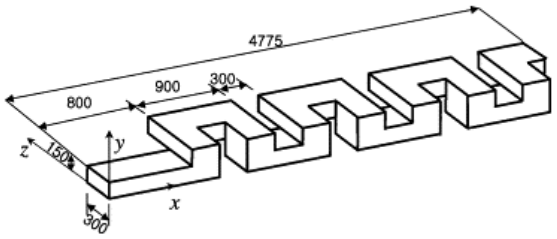

Figure 3: A three dimensional serpentine mixer, also using 90° turns (12).

A mixer that looks similar to this but utilises two channels is in figure 5 (14). This shows that infinitely complicated structures can be designed from basic shapes to form passive micromixers.

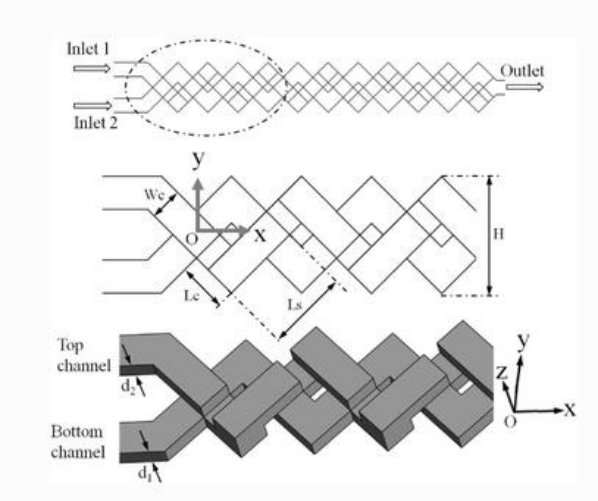

Figure 5: Schematic presentation of a micromixer with two crossing channels (14).

A planar mixer is shown in figure 6 where the segments of the main channel are connected by smaller channels called perforations (15). When the liquid streams move through the main channel the openings of the perforations are wetted. Since at the other side air is present, the liquid does not leave the perforations yet. This happens when the liquid has moved through the main channel and has wetted the other opening as well. As the liquid streams keep flipping, this mixing is very efficient with a mixing time of 0.4 s. The major limitation of this system is that the injected volume should not exceed the internal volume of the mixer making it unsuitable for continuous flow systems.

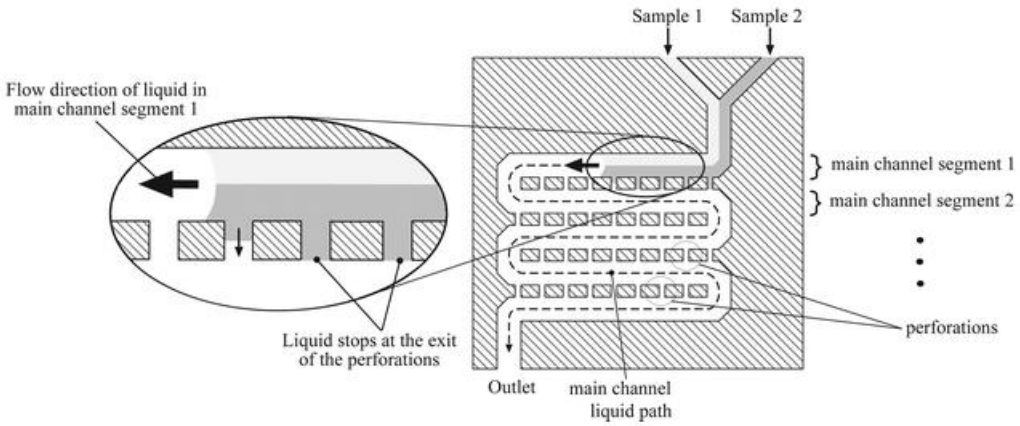

Figure 6: Planar passive mixer with small channels connecting the segments of the main channel. Two samples streams injected in the main channel for demonstration (15).

The mixing structure chosen in this study was the staggered herringbone chaotic mixer as shown in figure 7 (16). The efficiency of mixing depends on the asymmetry of the herringbone structures. The mixer was proven to work for systems with Reynolds numbers between 0 and 100 as well as for a broad range of flow rates.

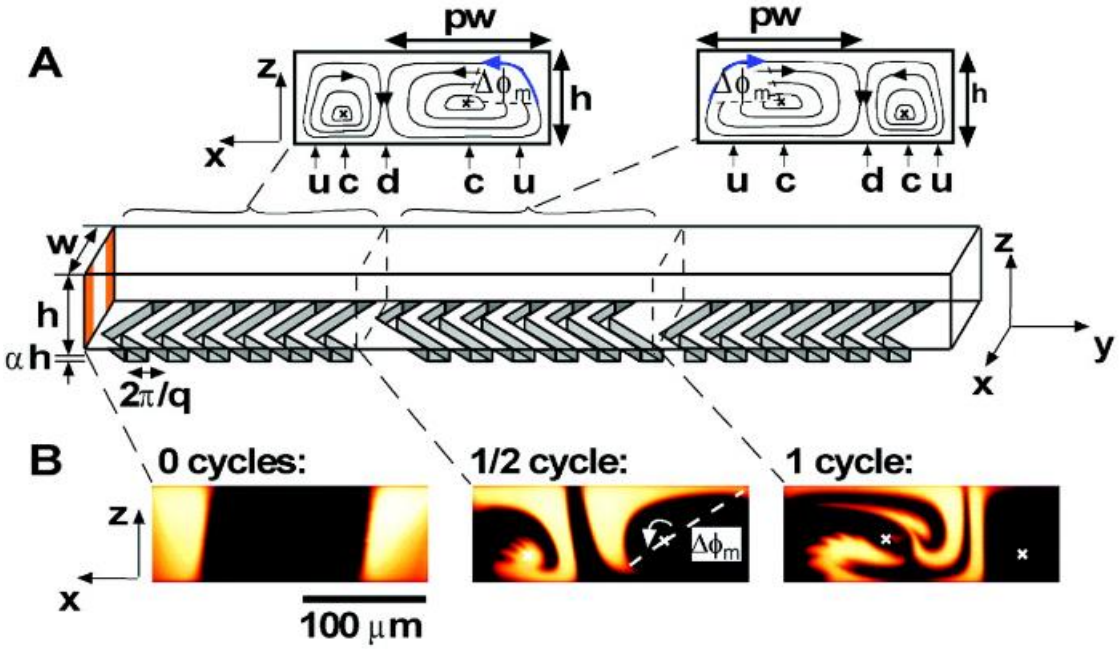

Figure 7: A: schematic presentation of 1.5 cycles of the staggered herringbone mixer and the schematic streamlines of the liquids through the mixer above; B: micrographs of the vertical cross sections after 0, 0.5 and 1 mixing cycle demonstrating a fluorescent liquid mixing with colourless liquid (16).

Salicylic Acid and Acetylsalicylic Acid

Salicylic acid (SA) or 2-hydroxybenzoic acid is a plant hormone responsible for regulating plant growth and development as well as protection against diseases (17). Historically salicylates have already been used in herbal medicine since several hundred years BC as it is found in a variety of plants such as willow bark. In humans, SA weakly inhibits cyclooxygenases 1 and 2 (COX 1, 2) (17). These enzymes are responsible for prostaglandin production, which are inflammatory mediators, leading to pain, fever and inflammation. SA was found to inhibit high-mobility group box 1, whose secondary function is as a damage-association molecular pattern. Via this pathway, it increases cytokine expression and inflammation. SA also inhibits glyceraldehyde 3-phosphate dehydrogenase (GAPDH). GAPDH plays a neurodegenerative-disease-associated role in the cell death cascade. SA binds GAPDH so it cannot move to the nucleus to induce cell death (17).

Acetylsalicylic acid (ASA) or better known as Aspirin, is a medicine that is given to treat pain, fever, inflammatory diseases and in lower doses to inhibit platelet aggregation (18). Aspirin was brought onto the market by Bayer in 1899. It was developed to replace to salicylate medicines such as salicylic acid which gave severe stomach complaints. Next to the molecular pathways of SA, ASA strongly irreversibly inhibits COX1 and 2, thereby inhibiting inflammation. The characteristic of ASA that sets it apart from the other salicylates is its ability to inhibit platelet aggregation. Due to its strong inhibition of COX1, prostaglandin PGH_2 cannot be formed. PGH_2 is normally used by thromboxane synthase to produce TXA2, which is a vasoconstricting agent and inducer of platelet aggregation. Platelets cannot produce new COX enzymes causing the long duration of ASA induced platelet aggregation inhibition (19).

Aspirin is synthesised from salicylic acid and acetic anhydride as shown in figure 8. The synthesis is performed under the influence of an acid catalyst and heat.

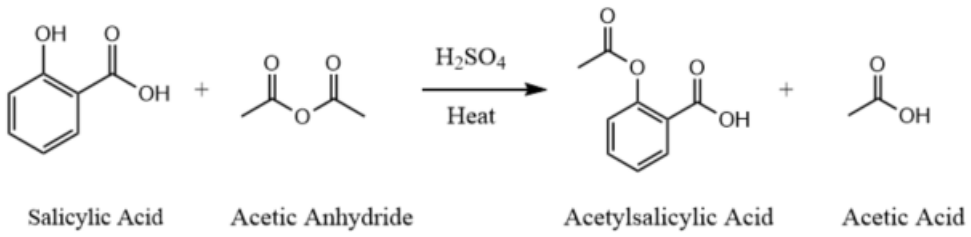

Figure 8: Synthesis reaction of salicylic acid and acetic anhydride to acetylsalicylic acid and acetic acid under influence of an acid catalyst and heat. Designed in ChemDraw.

Analysis Techniques

High performance liquid chromatography (HPLC) is one of the most used and strongest separation techniques for analysis in organic chemistry and the pharmaceutical industry (20). It has a mobile and a stationary phase and it separates compounds from a mixture based on their polarity. In reverse-phase HPLC (RP-HPLC), the mobile phase is polar and the stationary phase is nonpolar. The more polar the compound, the faster it is eluted from the column. A measure for the polarity of a compound is given by its logP value. The logP is the partition coefficient of a compound between octanol and water. The preference for the uncharged form of a compound for either an aqueous environment or for an organic environment is described by this (21).

Infrared (IR) spectroscopy is used to determine the structure of a molecule (20). IR energy is shone through a sample and the absorption by bonds in the molecule is measured. Certain types of bonds and functional groups have characteristic absorbances that can be used for structural analysis.

Ultraviolet and visible light (UV-Vis) spectroscopy is also a widely known analysis technique (20). UV and visible light are shone through a sample and at a compound- and bond-specific wavelength, this light can excite an electron leading to absorption of light. The amount of absorption is related to the quantity of a compound present in a sample.

The melting point of a compound is the temperature in which the compound transitions from a solid into a liquid state as the molecules are able to leave the crystalline structure and behave more freely. This technique for determining the melting point can help in identifying a compound, as all compounds have a characteristic temperature at which this phase transition occurs. It can also be used to study purity of a sample. A pure compound has a very narrow range (1-2 °C) in which it goes from solid to liquid. For low-purity samples a broader melting range will be observed (22).

Justification

Production of pharmaceutical dosage forms is generally done in batch processes. The various steps are often done at different locations leading to relatively long manufacturing times of the products. Another disadvantage of this system is the vulnerability of the production chain to disturbances (23). The effect of a disruption at one location could lead to a block of the whole chain and a potential shortage of the pharmaceutical products. The principle of continuous flow production is that every synthesis and production step is done in the same system at a single location. The benefits of such a system is that it would be easily adjustable and that it could be upscaled or downscaled based on the demand. These systems will also produce less waste and require less energy compared to batch synthesis (24). The continuous-flow production could also be an answer to the increasing medicine shortages as the manufacturing time is decreased. There are continuous-flow modules being used that are the size of a kitchen fridge (25). However, in this study it was decided to work on microchips. A benefit of using chips is that the reaction conditions are accurately controllable and adjustable. Another advantage is the small volumes that are used during testing, making it a relatively inexpensive system for analysing a reaction thus reducing costs for research (26). Microchips also give the opportunity to do analysis during the reaction without needing to extract samples from the system. The choice for PDMS was made as the polymer is durable, compatible with most solvents and reaction conditions, and is not as expensive as other possible materials (27). The glass master used to produce the PDMS chips, is one of the largest advantages. It can be reused many times, thus making it possible to make the same chips every time.

The aim of this study was to investigate whether it is possible to synthesise acetylsalicylic acid on a continuous-flow microfluidic device. The efficiency of this system was compared to the batch system based regarding the yield, the purity and the SA content. Lastly, it was checked if the products met the criteria for aspirin as stated by the European Pharmacopoeia (28).

2. Material and Methods

2.1 Aspirin batch synthesis

Materials

The HPLC analysis was done using a Hitachi LaChrom Elite HPLC system consisting of a L-2130 pump, L-2200 autosampler, L-2300 Column oven, a L-2455 Diode Array Detector and a LiChrospher® 100 RP-18 (5 µm) LiChromCART® 125-4 column. For the UV-Vis analysis a VWR UV-3100PC spectrophotometer and 10mm quarts cuvettes were used. A Shimadzu IRSpirit, Fourier transform infrared spectrophotometer was used for IR-analysis. The oxygen plasma set-up used contained an Edwards vacuum pump, a Harrick PLASMA PLASMAFLO PDC-FMG and a Harrick plasma plasma cleaner. Whatmas glass microfibre filters, 7.0 cm were used during the vacuum filtration. The melting point analysis was performed using a Electrothermal IA9000 digital melting point apparatus. In the continuous-flow set-up ProSense NE-1000 syringe pumps, BD 1 mL Luer-Lok and BD 1 mL Luer-Slip syringes, Braun Sterican g2 blunt and injection needles, and 1.6 mm Ø Teflon tubing were used.

Chemicals:

Ethanol 96% v/v, Acetic acid glacial 100%, Ethyl acetate HPLC grade, Sulphuric acid ACS reagent 95-97%, Phosphoric acid 85%, Acetonitrile HPLC grade > 99% and Methanol absolute > 99.95% were obtained from Boom (Meppel, the Netherlands). Acetic anhydride reagent grade 99%, Salicylic acid reagent grade 99%, Acetylsalicylic acid reagent grade 99%, Ferric chloride reactant grade 97%, Dibasic sodium phosphate ACS reagent > 99% and perfluorooctyl trichlorosilane 98% were obtained from Sigma-Aldrich (Zwijndrecht, the Netherlands). Silicone elastomer base Sylgard™ 184 and Silicone elastomer curing agent Sylgard™ 184 were obtained from DOW Chemical Company (Terneuzen, the Netherlands). Monobasic sodium phosphate reagentplus > 99% was obtained from Acros Organics (Bleiswijk, the Netherlands). UP water was obtained from MilliQ filtration set-up.

Synthesis

The batch synthesis were performed according to a modified literature procedure (29).

Salicylic acid (4.98 g) was mixed with acetic anhydride (AA, 8.00 mL) in an Erlenmeyer flask. Sulphuric acid (H_2SO_4, 8 drops) was added to the flask. The flask was heated on a water bath at 95 °C for 15 min. Demi water (15 mL) was added, the flask was removed from the water bath and left to cool to room temperature on the bench. After 3 min, the flask was put on ice and left to crystallise for an hour. The formed solid was filtered on a Büchner funnel set-up with glass microfibre filter and washed twice with ice cold water (3 mL). The solid was transferred to a beaker and ethanol (EtOH, 10 mL) was added. The beaker was put on a water bath at 75 °C. Additional EtOH (3 mL) was added to fully dissolve the solid after 10 min. Demi water (10 mL) was added and the beaker was set to cool on the bench for 5 min. Afterwards the beaker was placed on ice for 20 min. To cool the mixture even further the beaker was placed on a bath with ice in spiritus and left to crystallise over 30 min. The obtained solid was again filtered and washed using vacuum filtration. The dried product was weighed and used in the analysis.

Iron(III)chloride test

To four glass test tubes, demi water (1 mL) was added. To tube 1, a small amount of SA was added. To tube 2, ASA was added. The synthesis product was added to tube 3. Tube 4 served as the blank so

nothing was added. A 1% $FeCl_3$ solution was made by dissolving $FeCl_3$ (0.108 g) in demi water (10 mL). 1 drop was added to each of the four tubes and they were shaken briefly.

HPLC Analysis

Around 0.010 g SA and ASA were weighed in a volumetric flask which was filled up to 10 mL with acetonitrile (ACN). 100 µL was pipetted into a new 10 mL flask and was diluted 100 times by filling up with ACN again. Solutions containing only SA, ASA and synthesis product were made in the same way. Phosphoric acid (0.5 mL) was added to UltraPure (UP) water (1 L). The following ratios water with H_3PO_4 to ACN were tested on separation and resolution: 60:40, 70:30, 80:20 and 40:60. The final HPLC eluent was made by adding UP water (700 mL), ACN (300 mL) and H_3PO_4 (0.5 mL) to a bottle and mixing.

HPLC samples were made as described previously but using around 0.020 g of each compound. The solutions for the calibration curve were made as described below.

Table 1: Pipetting scheme used for the HPLC calibration curve used for the batch analysis

Vial number	Volume ASA stock (µL)	Volume ACN (µL)
1	1000	0
2	800	200
3	600	400
4	400	600
5	200	800

The chromatograms were recorded at 237 nm during 10-min runs at room temperature with a flowrate of 1 mL/min. The calibration curve was made by plotting the peak area against the concentration. Linear regression was used to determine the ASA content of the synthesis product.

IR-Spectroscopic Analysis

First a background measurement was recorded by the IR spectrophotometer. Then the crystal was covered with some of the synthesis product. The probe on the machine was lowered and a IR spectrum of the sample was recorded. The measured spectrum was compared to literature spectra by the software. The closest matches were displayed with a similarity percentage. To test whether IR was suitable for quantitative analysis samples with various ratios of SA and ASA were prepared a described below. The solids were mixed using mortar and pestle starting at mixing 1:1 and doubling the amounts until all was mixed. Pure SA and ASA were also tested. All measured spectra were again compared to literature spectra and the similarity was analysed.

Table 2: Amounts of SA and ASA mixed and their intended ratios for testing IR as quantitative analysis method

Intended ratio	SA (mg)	ASA (mg)
80:20	160.8	41.4
60:40	120.2	82.3
40:60	77	118.8
20:80	43	168.2

UV-Vis Spectrophotometric Analysis

A 0.1 M phosphate buffer with pH 6.8 was made by dissolving monobasic sodium phosphate (3.085 g) and dibasic sodium phosphate (3.473 g) in UP water (500 mL). The pH was measured using a potentiometric pH-meter. SA (0.020 g) was weighed in a 10 mL volumetric flask which was filled up

with the phosphate buffer. The stock (100 µL) was pipetted into a new 10 mL flask and filled up with buffer again to achieve a 100 times dilution. The same was done for ASA. A UV-Vis spectrum was measured between 190 and 450 nm. The solutions were diluted an extra 10 times. The synthesis product was directly diluted a 1000 times by adding 10 µL to a 10 mL flask. UV-Vis spectra were measured for each solution.

Melting Point Determination

Lastly, the melting point of the product was determined. As a reference, pure ASA was analysed with the melting point machine next to the product sample. The machine was preheated to 130 °C; after this the temperature increased with 1 °C/min. The measurement was repeated, but the machine was preheated to 120 °C this time. The melting range of both product and pure ASA were recorded.

2.2 Microfluidic flow demo

A microchip with two inlets leading to reservoirs was used. From these reservoirs the liquid streams met in a meandering channel. Two syringes were filled with coloured water, blue and yellow. Each syringe was placed in a syringe pump and connected to the chip with tubing. A vial was placed under the outlet tubing to collect the waste. The various flowrates were tested to observe their effects are stated in table 3.

Table 3: The different flow rates tested for each solution.

Flowrate blue (µL/h)	Flowrate yellow (µL/h)
200	200
100	100
180	20
20	180
20	20

The syringe with yellow water was replaced with a syringe with mineral oil. The flowrates tested are listed in table 4.

Table 4: The different flow rates tested for the water and oil streams.

Flowrate blue (µL/h)	Mineral oil (µL/h)
100	100
500	500
800	800
1000	1000
1000	500

Both parts were repeated on a microchip with a staggered herringbone micromixer. Connection pieces made from needles were used to connect the tubes to the chip as the inlets were smaller.

2.3 Microfluidic chip design and production

Designing the Photomask

The channels were designed using CleWin3.0 layout software. The main channel and channels connected to the inlets were made 300 µm wide. The main channel was made 50,000 µm long and the inlet channels around 4,700 µm. The micromixer was made with 156 µm wide wells and 86 µm between each herringbone. Mix cycles were made by pasting six identical wells after each other followed by six wells flipped horizontally. This was repeated three times with around 300 µm

between each cycle. The mixer structures were placed on a second level. To make the later part of the main channel as deep as the mixer wells that part was added to the second layer as well. The inlets and outlets were created as circles with 750 µm radius. The final design is shown in figure 9 and 10 .

Figure 9: Design of one complete chip in CleWin3.0 with the base layer in purple and the added height structures in the second green layer.

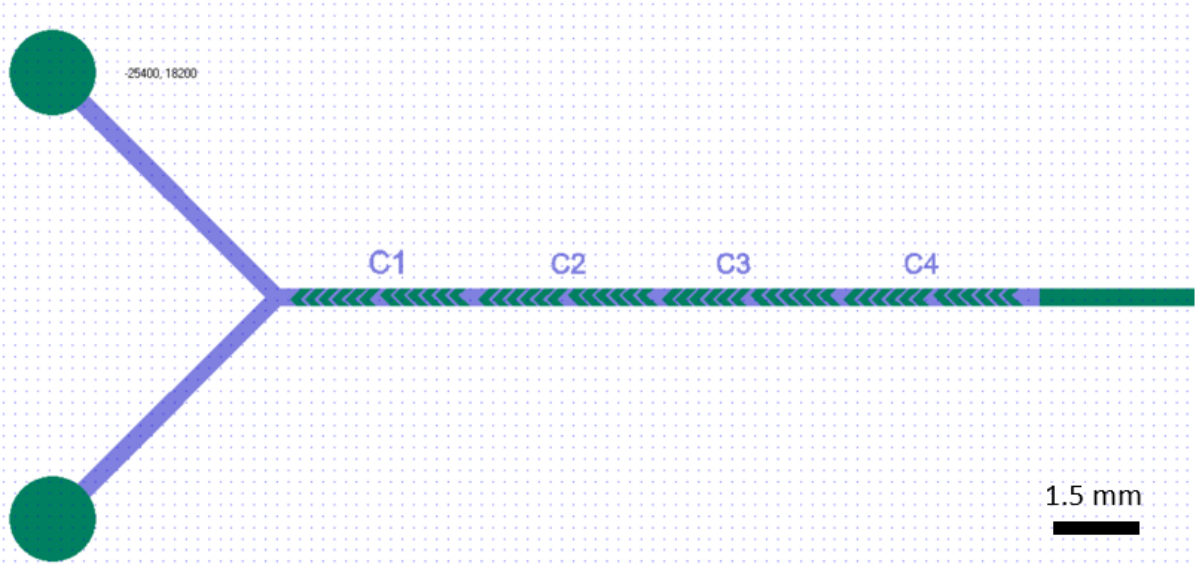

Figure 10: Close-up of the staggered herringbone mixer at the start of the chip.

Cleanroom protocols for glass master template

Specific programs and equipment specifications can be found in appendix 3.

In the clean room, a glass wafer was cleaned with acetone, isopropanol and UP water. The wafer was heated at 150 °C for 30 min to remove any water and cooled down. The wafer was placed on the spincoater and centred. SU-8 2025 (4 mL) was added to the middle of the wafer. The wafer was spun at 500 rpm for 10 s and then for 30 s at 1450 rpm. The wafer was soft-baked at 65 °C for 3 min and then at 95 °C for 7 min. The first photomask was placed on top and placed under a 365 nm UV-lamp. The wafer was exposed to UV for about 22 s. For the postexposure bake the wafer was baked at 65 °C for 2 min and at 95 °C for 6 min and then left to cool to room temperature. The SU-8 layer was activated with 20 s oxygen plasma treatment. The wafer was placed back on the spincoater and again SU-8 2025 was added. This time, the wafer was spun at 500 rpm for 10 s and at 1730 rpm for 30 s. This was baked at 65 °C for 3 min and at 95 °C for 6 min and then left to cool to room temperature. The second photomask was aligned and the wafer was exposed to UV light for around 20 s. The post-exposure bake was repeated as described above. The wafer was placed in a Petri dish with SU-8 developer for 2 min while shaking it. Then it was placed in fresh developer for 8 min. The wafer was rinsed with isopropanol and then dried and placed in a Petri dish. For the hard bake, the wafer was placed on a 150 °C hotplate for 20 min and then passively cooled to 65 °C. The last step was

silanization of the master template by incubating with 10 µl perfluorooctyl trichlorosilane in a vacuum desiccator for 30 min.

Chip production

Silicone elastomer base (51.23 g) was weighed in a plastic cup. Curing agent (5.35 g) was added in approximately 1:10 ratio. This was mixed for 2 min. The mix was then placed in a vacuum desiccator for 30 min to remove all air bubbles. The master was taped around the edges to a sheet of aluminium foil. The foil was folded up to form a bowl around the mould. The degassed silicone mixture was poured onto the master and placed on a heating plate at 70 °C for two hours. The PDMS layer was removed from the template. The individual chips were cut out using a scalpel. Holes were punched into the chips at the inlet and outlet sites using a 1.5 mm biopsy puncher. A chip with the channels facing up was placed on a glass plate together with a glass microscope slide. Both were placed in the plasma cleaner for about 25 s at a pressure between 310-320 mTorr. Afterwards the plate was taken out of the plasma cleaner and the exposed sides of the microscope slide and the chip were put together to bind. This was repeated for each chip. The entire process was repeated twice to produce a total of 15 chips.

2.4 Synthesis on chip

Solution 1 was made with acetic anhydride (1 mL) with H_3PO_4 (10 µL). A 250 µL glass syringe was filled with this solution 1. SA (circa 1.38g) was dissolved in EtOAc (10 mL) to get solution 2 (30). A glass 1 mL syringe was filled with the solution. After this the syringes were placed in the pumps, the diameter was set correctly and the flowrates were set to 4.13 µL/min for syringe with solution 2 and 0.87 µL/min for the syringe containing solution 1, resulting in a total flowrate of 5 µL/min. The syringes were connected to a chip with a staggered herringbone mixer along the entire length using tubes and needle connection pieces. A piece of tubing of 14.7 cm was connected to the outlet to achieve a reaction time of 15 min with a flowrate of 5 µL/min. A collection vial was placed at the end in an ice bath. The ice bath was used to cool the synthesis product and stop the reaction if it were to proceed at room temperature. The chip was placed above a water bath at 90 °C. A calibration curve was made by dissolving SA or ASA (circa 0.04 g) in ACN to make a 10mL solution. The solution was diluted 100 times by pipetting 100 µL in a new 10 mL volumetric flask which was filled up by ACN. The calibration curve was made with concentrations between 0.04 and 0.008 mg/mL as described in table 5. The calibration curve was measured using the HPLC method designed previously, runs of 7 min were recorded instead of 10 min. The solutions and calibration curve were remade each day.

Table 5: Pipetting scheme for the dilution curve used for this experiments and the following.

Vial number	SA or ASA dilution (µL)	ACN (µL)	Concentration (mg/mL)
1	1000	0	0.04
2	800	200	0.032
3	600	400	0.024
4	500	500	0.02
5	400	600	0.016
6	200	800	0.008

This experiment was repeated on a water bath of 60 °C.

Reaction times of 5, 7.5, 10, 15, 20 and 25 min were tested. For some the flowrates were changed and for the longer ones the length of the tube at the outlet was increased. For solution 2, the syringe was changed to a 10 mL glass syringe.

Table 6: An overview of which flowrates and length of incubation tubing used for each reaction time measured.

Reaction time (min)	Flowrate SA/EtOAc (µL/min)	Flowrate AA/H_3PO_4 (µL/min	Tubing length (cm)
5	12.3	2.7	14.7
7.5	8.2	1.8	14.7
10	6.15	1.35	14.7
15	4.13	0.87	14.7
20	4.13	0.87	19.7
25	4.13	0.87	24.7

Samples were made by pipetting 1 µL product into a vial containing either 99 µL EtOH or ACN. After the first measurement this was changed to 1 µL in 999 µL solvent.

The set-up was changed so that the incubation tubing connected to the outlet could hang under the chip holder and could get heated properly. Two holes were drilled in the chip holder and needles were put through to which the tubing could be connected. The solutions and calibration curve were made again. A piece of tubing of 19.7 cm was connected under the chip holder to test the reaction progression with a reaction time of 20 min.

The water bath temperature was lowered from 60 °C to 55 °C. Reaction times of 25, 30 and 40 min were tested. For 30 min 29.7 cm tubing was used and 39.7 cm for 40 min.

Reaction times of 50, 60, 90, 120 and 180 min were tested the next days. For each minute increase in reaction time the length of the incubation tubing was increased by 1 cm leading to 179.7 cm for 180 min.

180 min was tested again and samples were taken at the outlet at t=0, t=15, t=30, t=45 and t=60. A different calibration curve was made. SA (0.04 g) was weighed in a 10 mL volumetric flask. The flask was filled up to 10 mL with ACN. This was diluted 20 times by pipetting 0.5 mL of stock into a new 10 mL flask which was filled up with ACN. The concentration range of the calibration curve was 0.2-0.01 mg/mL. This calibration curve was remade every following day.

Table 7: Pipetting scheme for new calibration curve with a higher concentration range to include the sample concentrations.

Vial number	SA or ASA dilution (µL)	ACN (µL)	Concentration (mg/mL)
1	1000	0	0.2
2	800	200	0.16
3	600	400	0.12
4	400	600	0.08
5	200	800	0.04
6	100	900	0.02
7	50	950	0.01

Based on previous results the acid catalyst was changed from H_3PO_4 to H_2SO_4 and was added to solution 2 instead of solution 1. Also the glass syringe for AA was changed to a 1 mL plastic syringe. The experiment for testing consistency of the system was repeated.

To visualise the reaction progress over time a set-up was build similar to the previous one with a total tubing length of 179.7 cm for a reaction time of 180 min. However starting from the end, 30 cm segments were cut off till a sixth segment of 29.7 cm remained. Needles were cut and used to connect all the segments again. This created the opportunity to collect samples of different reaction times in the same system. The reaction times tested were 180, 150, 120, 90, 60, 30 and 0 min. For 0 min samples were taken right after the chip when the mixing had occurred. This was repeated using 179.7 cm of intact tubing. For taking the samples segments of 30 cm were cut off using a scalpel starting from the end. After cutting off a part of the tubing, product was collected for 2 min before cutting off another piece.

The last test was done to collect a larger amount of product for purification. Tubing of 359.7 cm was cut and the flowrates were set to 12.39 µL/min for solution 2 and 2.61 µL/min for solution 1. With a total 15 µL/min flowrate the reaction time was 2 h. The product was collected in the syringe in the withdrawing pump, during approximately 4 hours.

The product was transferred to a glass vial with the cap left off. It was placed on top of the water bath to enhance the evaporation of EtOAc. The vials were stored in a freezer at -20 °C over the weekend. The product was poured on a filter on a Büchner funnel vacuum set-up. The vial was washed twice with cold water (3 mL). The solid on the filter was transferred to a beaker and EtOH (1.5 mL) was added. The beaker was placed on a 65 °C water bath until the solid fully dissolved. Water (1.5 mL) was added to the beaker. The beaker was left to cool on the bench for 10 min before it was placed on an ice bath. After 30 min the beaker was placed on a colder ice bath with spiritus. More water (5 mL) was added in segments. This mixture was placed back in the -20 °C freezer overnight.

The vial was taken from the freezer and left to thaw on the bench. The product was filtered on a Büchner funnel. After 5 min the solid was transferred to a glass vial and weighed. For the HPLC sample product (0.0214 g) was weighed in a 10 mL volumetric flask. The flask was filled up with ACN. This solution was diluted 10 times in a new 10 mL flask. This dilution was directly measured in the HPLC.

3. Results and Discussion

3.1 Aspirin batch synthesis

After the synthesis and purification steps white flaky crystals were obtained which smelled faintly like vinegar. This could be caused by the decomposition of ASA into SA and acetic acid in the presence of left-over water. The obtained product had a mass of 4.99 g. This translated into a yield of 81%.

Iron(III)chloride-test

The first test done with the obtained synthesis product was the iron(III)chloride test to qualitatively determine the purity of the product. The $FeCl_3$ gave a dark purple colour in presence of SA and stayed colourless with pure ASA (figure 11). The mix in the product tube stayed colourless and only when holding the tube in the light an almost invisible purple hue could be observed near the meniscus. This slightly purple hue could indicate that a very small amount of SA was present in the product on the batch synthesis.

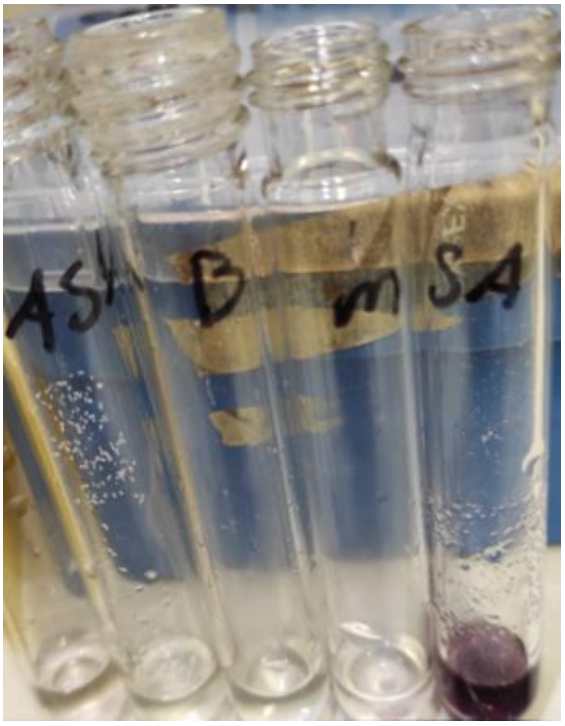

Figure 11: Results of the $FeCl_3$-test. Order of the tubes: Pure ASA (reference); blank; the batch synthesis product; pure SA (reference).

HPLC analysis

The raw data for the HPLC measurements for this section can be found in appendix 2.1

Then HPLC analysis was used. First the optimal eluent was determined. With ratio 60:40 of water to ACN ASA was eluted at 2 min and 3 min. The peaks showed no overlap but were quite close to each other. For good qualitative and quantitative analysis it is essential that the peaks are completely separated as was the case. Small variations in the conditions of the HPLC machine and the solutions have influence on the elution. To ensure these would not cause the peaks to overlap in later measurements, a stronger separation was desired. A ratio of 70:30 eluted ASA at 3.1 min and SA at 4.6 min. This gave two clear and separated peaks with good resolution. The only type of distortion of the peaks was some tailing for the ASA and SA peaks for each eluent. Tailing is often caused by ionised silanols from the column interacting with the eluent and analyte. Methods to prevent tailing are by buffering the eluent, lowering the pH or using end-capped columns (31). Generally, tailing

decreases the accuracy of using the peak area for quantitative analysis. Ratio 80:20 eluted ASA at 6 min and SA at 10 min. The longer elution times did not increase the resolution nor did it give better separation and was therefore determined unnecessary and considering optimisation of analysis time undesired. 40:60 led to elution times at 1.4 min and 1.7 min making the two peaks overlap. Overlapping peaks are not suitable to use for quantitative analysis as the peak area cannot be determined accurately. The ratio of 70:30 water to ACN with 0.5% H_3PO_4 was chosen as the best eluent.

While measuring a spectrum for a sample that was prepared the day before, it was observed that the SA and ASA had degraded overnight almost completely into different unidentified compounds. It is hypothesised that it might be due to ACN. From this, it was concluded that fresh samples should be made again every day.

A calibration curve was made plotting the AUC against the concentration of ASA (figure 12). The R^2 of the trendline was 0.9887 which was deemed acceptable though not as high as the desired 0.995. This would indicate that 99.5% of the variability of the data is explained by the model. Using the trendline equation $y=5*10^7x + 56494$ and the AUC of the ASA peak obtained for the synthesis product the ASA concentration was determined. This was calculated to be 0.0211 mg/mL. Compared to the theoretical concentration of 0.0218 mg/mL the purity of the product was estimated to be 97%.

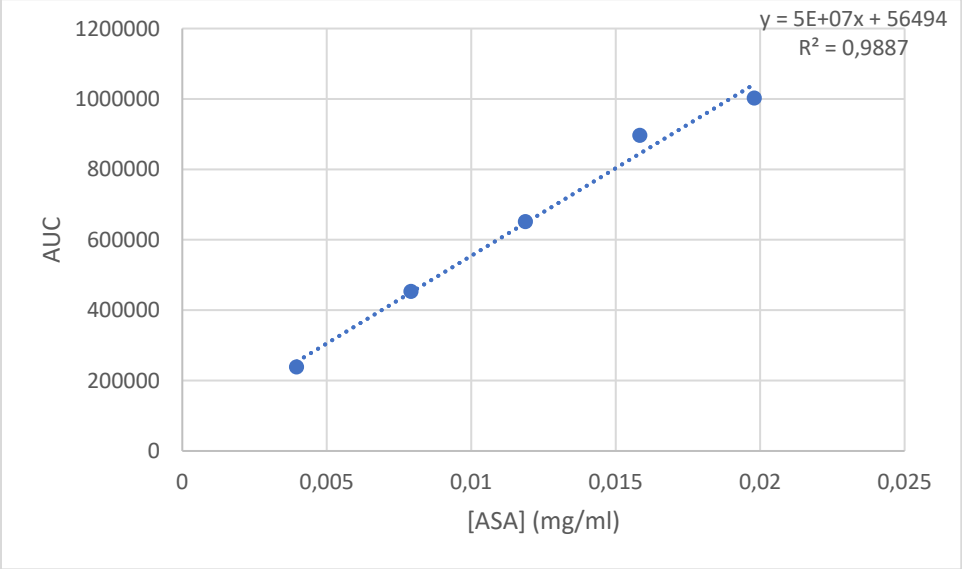

Figure 12: Calibration curve as measured for the analysis of the batch synthesis based on figure S4

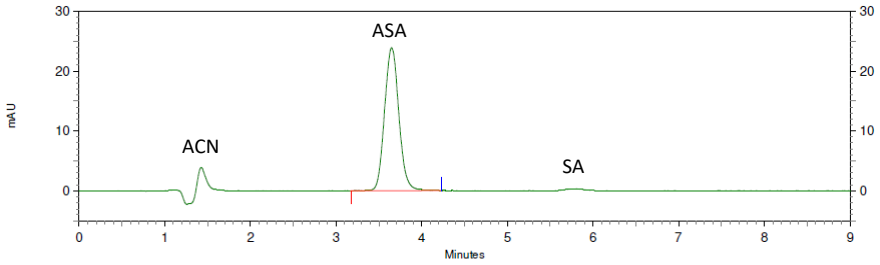

DAD-CH1 237 nm Results

Retention Time	Area	Height
3.647	1113081	95427
Totals		
	1113081	95427

Figure 13: Chromatogram of the synthesis product with a clear peak at 3.6 min, indicating the presence of ASA in the sample. No peak was measured at 5.8 min, meaning that no SA or a negligible amount was present in the batch product.

Figure 13 shows that the retention times of ASA and SA had significantly shifted from 3.1 to 3.6 min and 4.6 to 5.8 min respectively. This is undesired, as with more complicated mixtures identification of the compounds would become more difficult. Other troubles with the HPLC machine were an unstable baseline and tailing independent of the eluent. These phenomena lead to less accurate AUC values or peak heights, thus to a less accurate quantitative determination. The HPLC column was thoroughly washed using a gradient elution with a steadily increasing ACN concentration. Many peaks were detected during the washing indicating that a lot of debris was stuck on the column and was only now eluted. It could be that these compounds interfered with previous recordings. After the washing, the problem of the unstable baseline was solved, but the tailing persisted.

UV-Vis Spectrophotometric Analysis

The spectrum of pure SA showed a high peak at 209 nm fused with a lower peak at 230 nm and a separate peak at 296 nm (figure 14A). Pure ASA only showed a peak at 201 nm (figure 14B). In the spectrum of the batch product only the peak at 201 nm is visible which matches the ASA spectrum (figure 14C). This would indicate that if compounds other than ASA were present, their concentrations were too low to be detected in this dilution. It could also be that impurities were present that did not have any absorbance in the measured UV range. The last option is, that there are impurities that do have UV absorbance, but around the same wavelength as the ASA peak. This would make it impossible to detect with this analysis technique. Based on the UV-Vis results it cannot be concluded whether the batch product was pure, only that ASA was present.

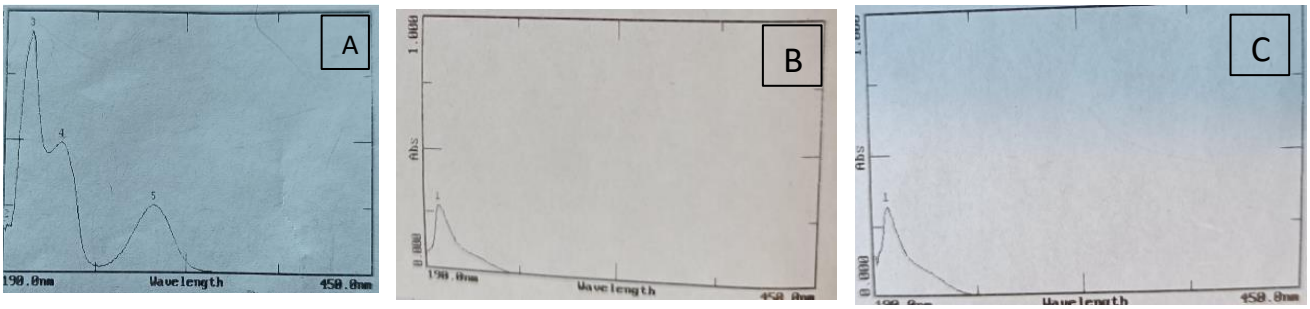

Figure 14: UV-Vis spectra measured for 190-450 nm. A: pure SA (reference); B: pure ASA (reference); C: batch product.

IR-Spectroscopic Analysis

IR spectrometry was used identify the main compound in the synthesis product and obtain an estimate on the purity. Comparison with literature spectra showed a 96% similarity of the product to

ASA (figure 15). This would indicate that 96% of the recorded peaks were due to ASA and only 4% was due to other compounds. Based on this it could be hypothesised that the batch product had a high purity. However, since the signals of various compounds can overlap and not be recorded as separate peaks, it could not be assumed that this directly meant a purity of 96%.

Various known ratios of SA to ASA were tested to analyse whether IR would be suitable as quantitative analysis method. IR only showed the compound with the highest similarity (table 8). This would make it impossible to analyse the presence of multiple compounds. Only for the ratio 40:60 SA to ASA, the literature search matched both the compounds. ASA had a similarity of 89% and SA of 82%. Even though the ASA content of the sample was significantly higher than the SA content, this was not reflected as much in the similarity percentages. For the samples that got matched to one compound, it could be observed that the similarity to the literature spectra decreased as the content decreased. However, this decrease was around 5% whereas the content dropped with 40%. No proportional linear relationship could be observed. This could be due to the fact that the molecules of SA and ASA were too similar and therefore most of the spectrum would match regardless of which was present more. IR-spectroscopy records absorbance of IR radiation by molecular bonds. The wavelength of the radiation absorbed is determined by the vibration frequency of the bond. This vibration is characteristic to specific types of bonds and groups in a molecule (20). As the molecular structure of SA and ASA are the same for most part, it would also be expected to obtain similar IR-spectra for both compounds. This made IR spectroscopy an unsuitable method for quantitative analysis.

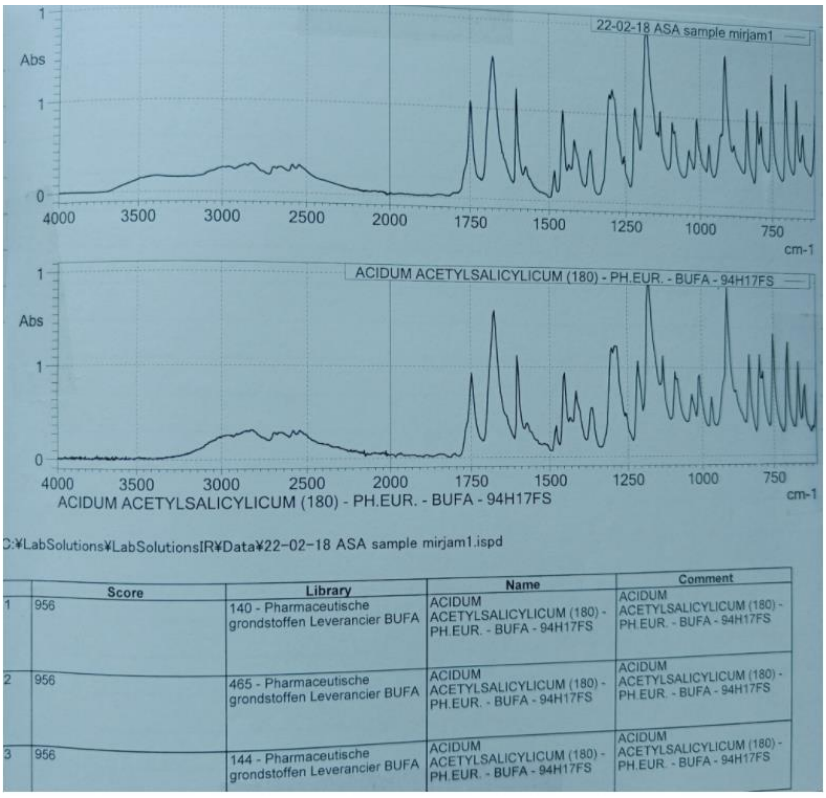

	Score	Library	Name	Comment
1	956	140 - Pharmaceutische grondstoffen Leverancier BUFA	ACIDUM ACETYLSALICYLICUM (180) - PH.EUR. - BUFA - 94H17FS	ACIDUM ACETYLSALICYLICUM (180) - PH.EUR. - BUFA - 94H17FS
2	956	465 - Pharmaceutische grondstoffen Leverancier BUFA	ACIDUM ACETYLSALICYLICUM (180) - PH.EUR. - BUFA - 94H17FS	ACIDUM ACETYLSALICYLICUM (180) - PH.EUR. - BUFA - 94H17FS
3	956	144 - Pharmaceutische grondstoffen Leverancier BUFA	ACIDUM ACETYLSALICYLICUM (180) - PH.EUR. - BUFA - 94H17FS	ACIDUM ACETYLSALICYLICUM (180) - PH.EUR. - BUFA - 94H17FS

Figure 15: IR spectrum for the batch product with literature matches as provided by the software.

Table 8: Literature matches as provided by the software for various ratios of SA:ASA. Raw data can be found in appendix 2.2

SA (%)	ASA (%)	System match	Similarity (%)
100	0	Acidum salicylicum	99%; 96%
80	20	Acidum salicylicum	97%; 93%
60	40	Acidum salicylicum	93%; 89%
40	60	Acidum acetylsalicylicum Acidum salicylicum	89% 82%
20	80	Acidum acetylsalicylicum	90%
0	100	Acidum acetylsalicylicum	96%

Melting point

The product sample and pure ASA reference were placed in the machine and it was preheated to 130 °C. The sample started to melt before the preheating was complete, indicating that its melting point was below 130 °C. The ASA reference started to show some signs of melting at 132.1 °C and was fully melted at 139.7 °C. The second run was started at 120°C and a melting range for the sample was observed at 128.8 – 129.7 °C. For ASA, the range was narrowed to 136.4 – 139.5 °C. The literature melting temperature of ASA is 135 °C. That the observed melting point does not match this could be due inaccurate calibration of the melting point machine. However, a relative broad melting range was seen for ASA where a melting point was expected as is characteristic for pure compounds. This could indicate that the ASA contained impurities that would increase the melting temperature. For the batch product sample, a quite narrow melting range was recorded. Usually this would be indicative of a pure compound. Since the melting point was lower than the literature value and the reference sample it could be assumed that this was not accurate for the product. Impurities that could lower the melting temperature were water and organic solvents used during the synthesis (20). When filling the sample tubes it was noticed that the synthesis product moved down the tube with more difficulty than the ASA. This could also be an indication that the product was insufficiently dried and water or solvent remained. The melting range and temperature seemed to contradict each other concerning the purity of the synthesis product.

In general the analysis of the product showed a purity of 96-97% and an very small amount of SA present. Purified aspirin should contain 99.5-100.5 % ASA and the allowed amount of SA in a dose of ASA is 0.15% (28). The batch product does not meet the first criterion for the ASA content. The SA content of the batch product was not determined quantitatively, so no conclusion could be drawn regarding the second criterion.

3.2 Microfluidic flow demo

With equal flowrates of the yellow and blue water solutions the lanes on the chip were the same width. For flowrates of 200 µL/h, the lanes stayed separate and only near the outlet a green interface was observed. For 100 µL/h, a wider green interface was observed and with 20 µL/h this occurred halfway on the chip already and near the outlet only very thin lanes of blue and yellow could be seen but majority of the liquid was green. At a 100 µL/h flowrate for both, oil and water went through the chip in alternating bubbles. With 500 µL/h, water seemed to stick to the channel walls in bubbles with oil filling the rest of the channel. At 800 µL/h, the blue water bubbles could be seen moving along the channel, but were still sticking to the wall. With 1000 µL/h the water bubbles started to connect to each other. Setting the water to 1000 µL/h and the oil to 500 µL/h seemed to create two even streams for the oil and water that could be seen flowing alongside each other.

The mixing efficiency of the staggered herringbone mixer was tested. At the higher flowrates the blue and yellow solutions were almost completely mixed after two cycles of 12 wells each and completely mixed after the third cycle. For the total flowrate of 40 µL/h complete mixing was achieved during the second cycle. For oil and water, the mixer had not much effect. The oil and water went through the chip in alternating bubbles. The bubbles seemed to get smaller with lower flowrates.

Based on the observed effectiveness it was decided to design a chip with a staggered herringbone mixer of four cycles of 12 wells each to ensure complete mixing, but also allowing the latter part of the channel to be deeper.

3.3 Master template and Chip production

Figure 16 shows the master template for the PDMS chips as produced in the clean room. It can be seen that the two layers not were precisely on top of each other. Due to the absence of the usual equipment for placing the layers correctly it had to be done by bare eye making it difficult. However, since the layers were still connected it was assumed that the functionality of the chip was unaffected. The slight misalignment was visible in the close-up photos in figure 16 taken with a microscope. Figure 17 shows the mixer and the channels in the finished PDMS chips.

The Reynolds number for the microsystem used in this study was estimated to be 0.92 using the right equation in figure 2 (appendix 1). The calculations were made with the assumption of circular channels, based on the main flowrate (5 µL/min) used and only considering the viscosity of the main component ethyl acetate (32).

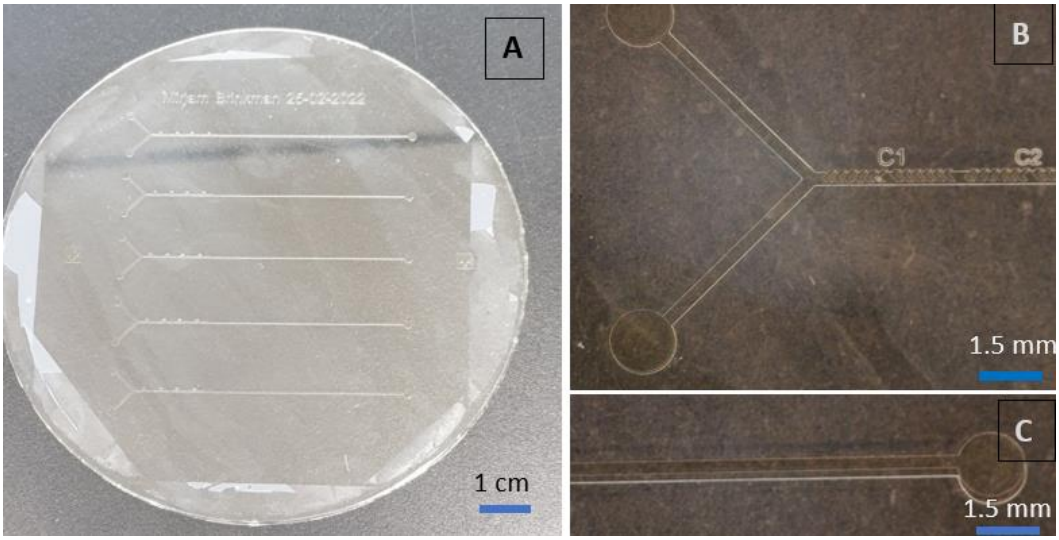

Figure 16: A: the final master template for the PDMS chips as produced in the cleanroom; B: shows a close up of the inlets the staggered herringbone micromixer; C: shows a close up of the outlet and the last part of the main channel.

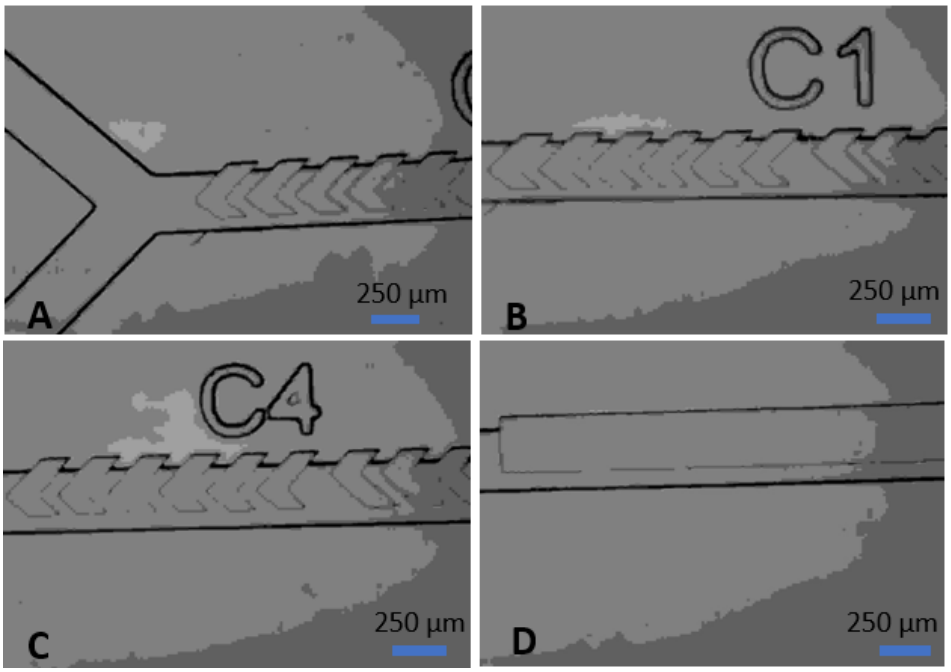

Figure 17: Photos taken with a microscope of the finished PDMS chips. A, B, C: the first and the fourth mixing cycle of the staggered herringbone mixer, with visible misalignment. D: Straight part of the main channel with also misaligned layers.

3.4 Synthesis on chip

In this section all the results obtained for various prototypes and subsequent adjustments to this system are presented and discussed. All calibration curves used for analysis can be found in appendix 4.1. Other relevant curves that were not placed in the results section can be found in appendix 4.2.

3.4.1 Synthesis prototype 1

For this first prototype, the water bath was set to 90 °C as was used in the batch synthesis. The same molar equivalents for SA, AA and acid catalyst were used as in the batch synthesis. Phosphoric acid was used as acid catalyst instead of sulphuric acid as it is easier to remove from the product (30).

Figure 18: Prototype 1 containing 2 syringe pumps; Tubing connecting the syringes to the chip inlets; The chip on a 90 °C water bath; Incubation tubing going from the chip outlet to the collection vial on an ice bath.

A reaction time of 15 min was tested with a flowrate of 5 µL/min. The product was collected in a vial on an ice bath to stop the reaction. The product did not leave the chip with the expected rate and bubbles were observed in the incubation tubing and on the chip. This was probably due to EtOAc evaporating on the chip as its boiling point is 77 °C and the chip temperature was around 82 °C (33). Figure 19 shows a white solid at the end of the syringe for solution 2. This leakage could be due to damage in the syringe preventing it from fully closing or the presence of gas in the chip caused an increase in pressure for the liquid going into the system and to release the pressure the solution was pressed out at the back instead. The channels of the chip are clearly visible in figure 19 indicating that they are filled with gas.

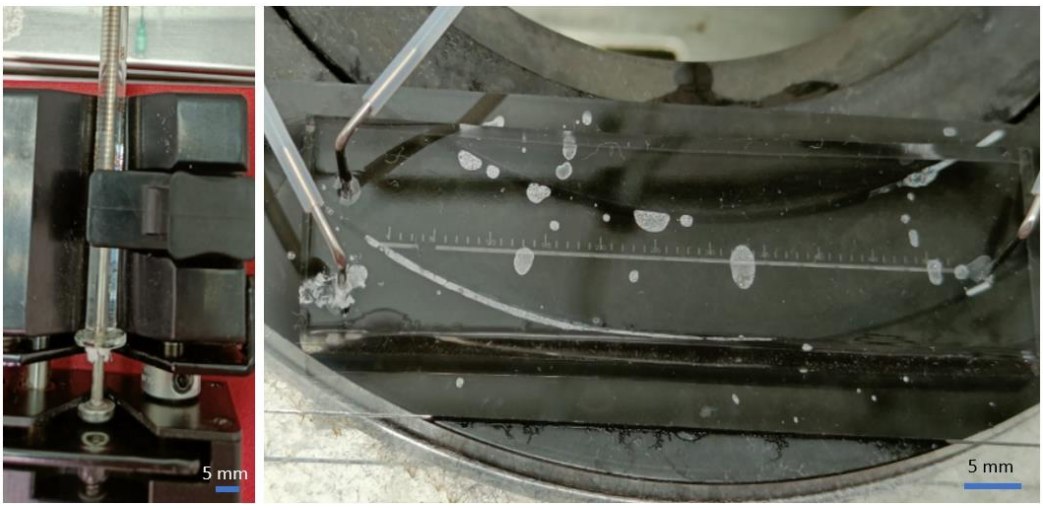

Figure 19: On the left, the syringe used for solution two with solid formed at the back; on the right the microchip with a gas-filled channel.

3.4.2 Synthesis prototype 2

The water bath was set to 60 °C based on the previous observations of EtOAc evaporation. The syringe containing solution 2 was replaced by a new one to rule out that the problem was due to a leaking syringe. The various reaction times were tested and the chromatograms were placed in an overlay. The samples were diluted in ACN and EtOH. EtOH was used to break down excess AA via an esterification reaction, in case cooling was insufficient to stop the reaction (figure 21). Measurements of the same product in ACN and EtOH were compared. ACN was the preferred solvent as it was most similar to the HPLC eluent used. To eliminate the possibility of the reaction proceeding in the collected product EtOH was added to quench the reaction. The difference between the two solvents were analysed to determine whether this quenching was needed to obtain accurate results.

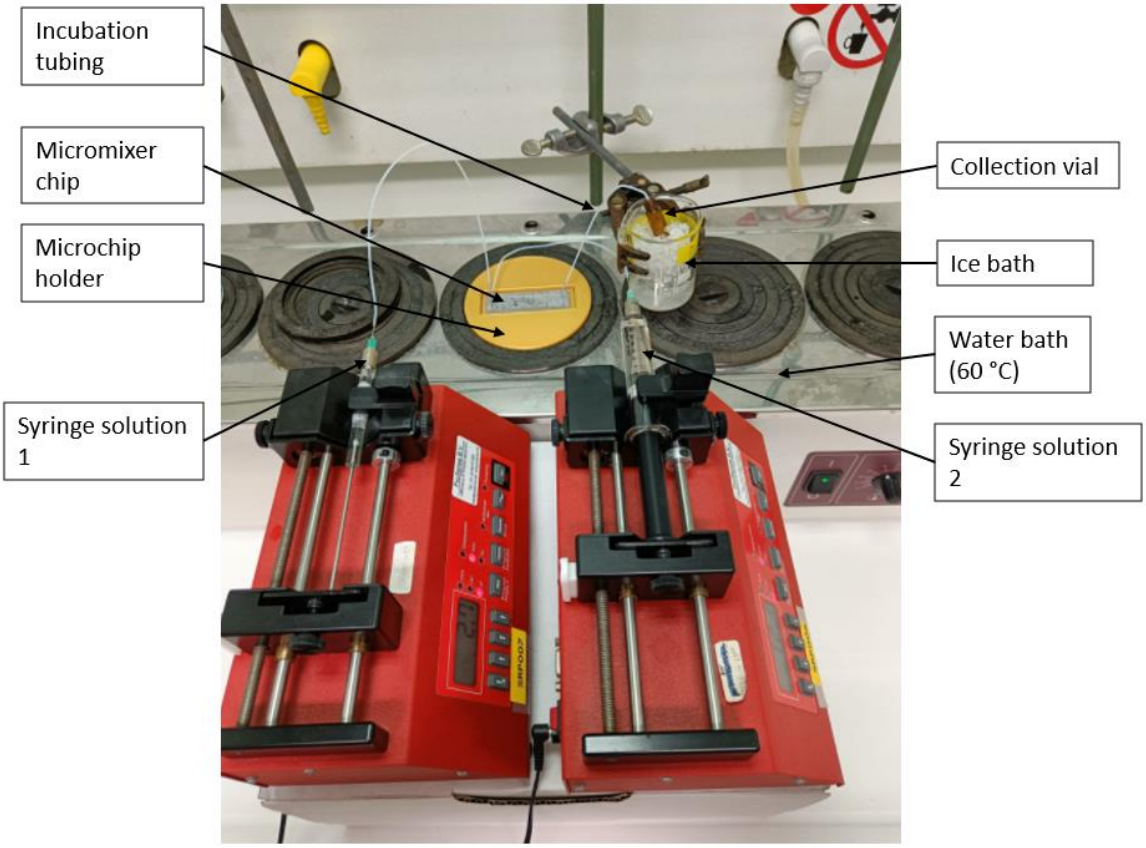

Figure 20: Prototype 2 with the following adjustments compared to prototype 1: A chip holder for stability, new syringe for solution two on the right and the water bath lowered to 60 °C.

Figure 21: Esterification reaction of acetic anhydride by ethanol to form acetic acid and ethyl acetate. Figure adapted from (34)

There seemed to be an issue with the flow through the system when using a flowrate of 5 µL/min as after 25 min no product was being collected. To test the system a total flowrate of 50 µL/min was

used. This gave a clear visible flow. It was decided to first test reaction times shorter than 15 min which used higher flowrates to check if the flow would stay constant. For the reaction time of 15 min a flowrate of 5 µL/min was used again, but this time the flow stayed constant.

In general it seemed that the SA peak around 4.5 min got slightly lower as the reaction time increased but this was not consistent (figure 22, 23). Figure 22 shows an overlay of the ACN samples. Here, the 15 min reaction gave the second highest SA peak and the lowest peak was for 7.5 min. For EtOH only the 20 min reaction time was unexpected as it gave a lower SA peak than 25 min (figure 23). The ASA peaks were hard to see as they were low and the baselines were not completely stable. The irregularity was also shown when the reaction time was plotted against the AUC of the SA and ASA peaks. As the AUC and peak height are proportional to the sample concentration this would indicate a fluctuating concentration. It was hypothesised that EtOAc was evaporating, making the concentrations of ASA and SA unreliable for monitoring the reaction progress. Instead the height ratio between the two peaks was considered. This ratio is independent of concentration and therefore the effect of the possible evaporation was eliminated. In the graph it is clear that the ratio increases as the reaction time increases (figure 24). However, it does not increase much, going from 0.02 to 0.09. The longest reaction time lead to a peak height of ASA that was only 9% percent of the SA peak height. This was much lower desired, as in optimal conditions SA should not or barely be present and ASA would the primary compound present.

As the incubation tubing at the outlet was above the chip, it was not actively heated. Due to the large surface area to volume ratio of the reaction mixture, it is likely that it was almost immediately cooled down to room temperature after leaving the chip. The small increase of only 7% peak height compared to SA suggests that the reaction proceeds very slowly at room temperature. Figure 24 shows no significant difference observed between product diluted in ACN or EtOH. As the calibration curves were also measured in ACN, it would be expected to get more accurate results for the ACN measurements. Therefore, only the data collected with ACN dilutions was considered.

Based on these observations the following adjustments were made. Two holes were drilled into the chip holder parallel to the chip and needles were cut and shaped to fit through. This made it possible to connect the incubation tubing at the bottom of the chip holder and have it hang above or in the water bath. To eliminate the evaporation of EtOAc the product was collected in closed HPLC vials in the next experiment using a sharp needle to pierce the cap. As the reaction was not proceeding significantly at room temperature it was decided to collect the product at room temperature and no longer on an ice bath.

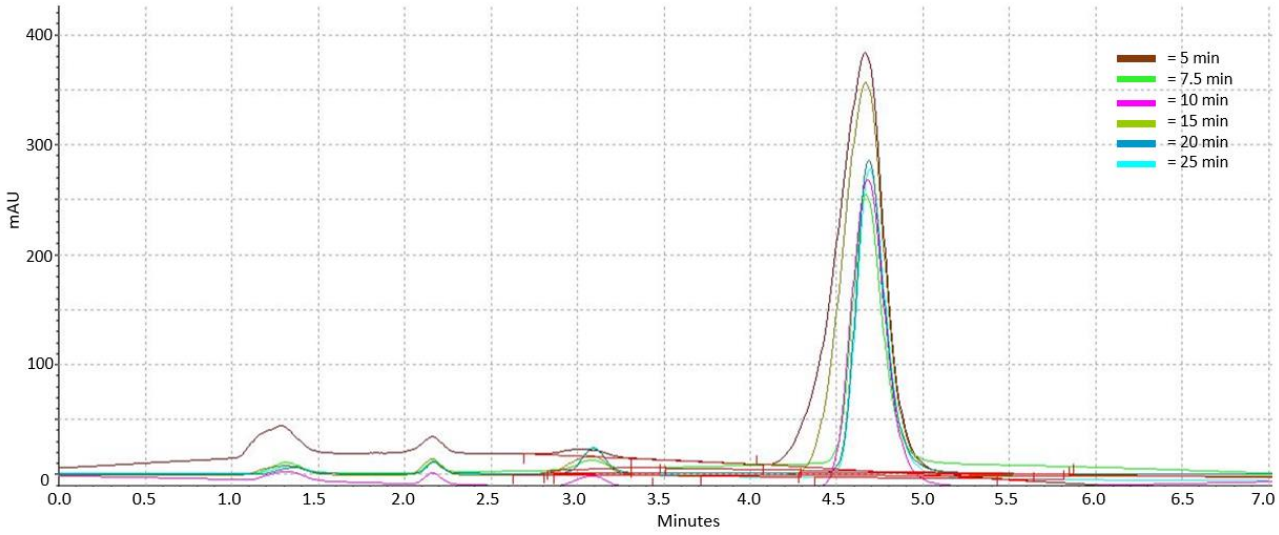

Figure 22: Overlay of the chromatograms measured for product diluted in ACN for the reaction times 5, 7.5, 10, 15, 20 and 25 min.

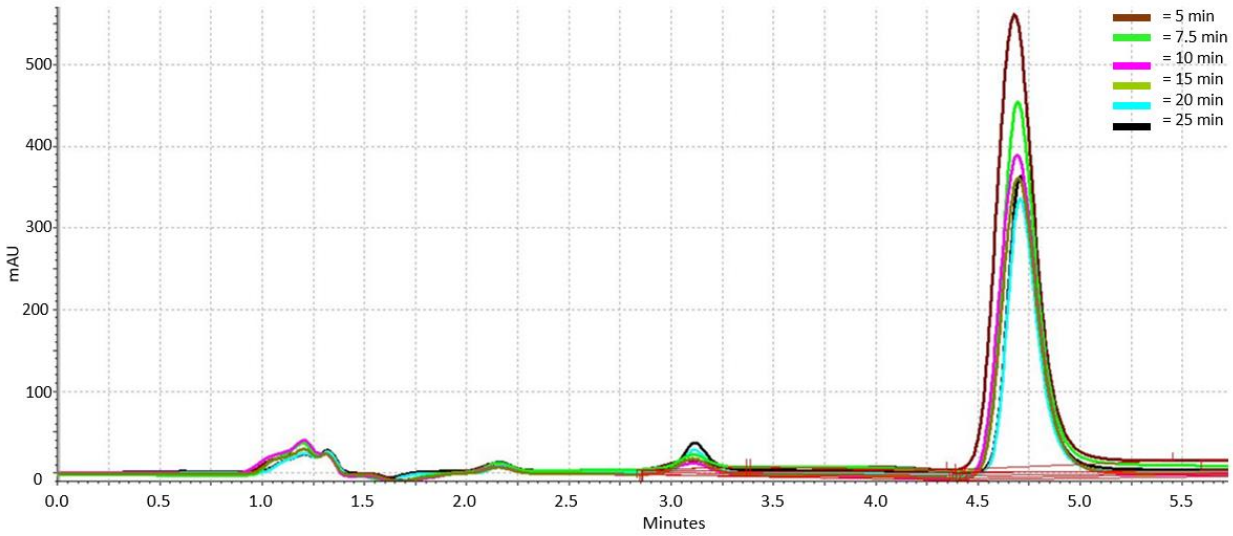

Figure 23: Overlay of the chromatograms measured for product diluted in EtOH for the reaction times 5, 7.5, 10, 15, 20 and 25 min.

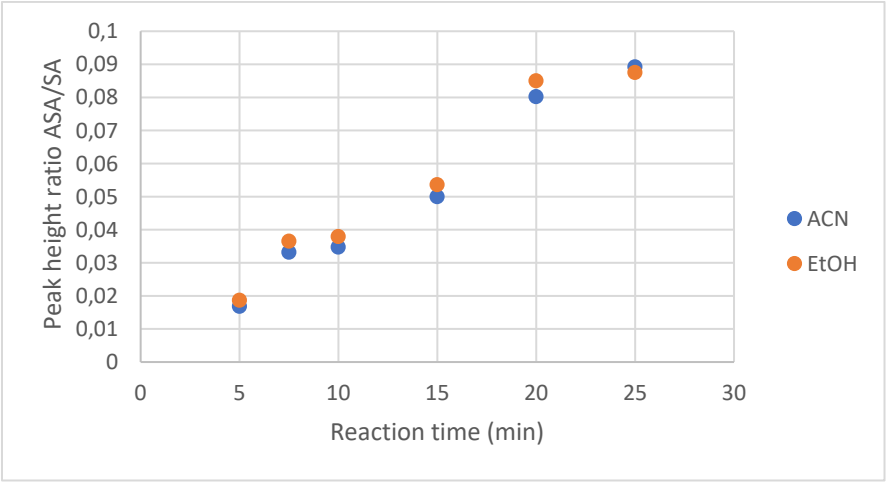

Figure 24: Graphical representation of peak height ratio of ASA to SA on the y-axis plotted against the reaction time of the product. Product diluted in ACN shown in blue and product diluted in EtOH in orange.

3.4.3 Synthesis prototype 3

In this prototype, the reaction mixture was heated properly during the entire reaction time. There was extra distance the reaction mixture had to travel in the system: the connection piece from the chip outlet to the needle, which connects to the start of the reaction tubing and the needle at the end connected to the collection vial (figure 25). As the reaction mixture is not heated in these parts and the reaction was shown to barely proceed at room temperature, the residence times of the mixture in these parts were neglected as part of the active reaction time.

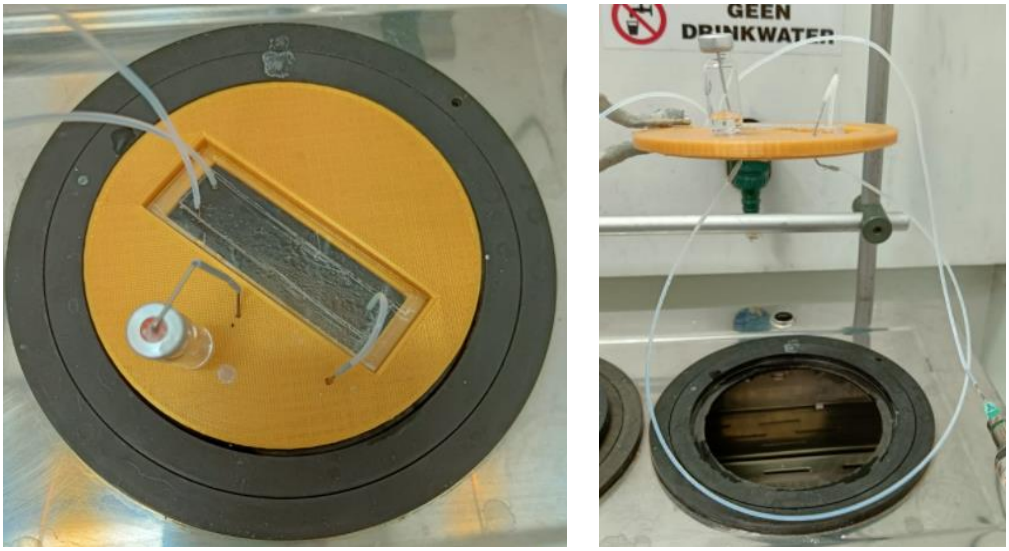

Figure 25: Prototype 3 with the proposed adjustments: on the left the capped HPLC vial with sharp needle for product collection and on the right the incubation tubing connected by needles underneath the chip holder.

The reaction was conducted at 60 °C again. The first reaction time to be tested was 20 min. After 40 min no product had been collected yet. The incubation tubing was checked and many gas bubbles were present again, similar to the first prototype were the reaction was performed at 90 °C. It was hypothesised that EtOAc was still evaporating at 60 °C. On the chip in the previous prototype this was not observed as the chip reaches a temperature of 10-15 °C below the water bath temperature. This was measured by holding a thermometer against the underside of the glass on the water bath. The temperature of the water bath was adjusted to 55 °C to keep the temperature as high as possible.

The reaction times of 20, 25, 30 and 40 min were tested. The channels and tubing were essentially free of bubbles at this new temperature. For the few bubbles that were present, it could not be stated whether they were still due to EtOAc evaporation or due to gases dissolved in the reaction solutions. The concentrations were calculated using the trendline equation of the calibration curve. Figure 26 shows typical calibration curves for SA and ASA. It was decided to use the peak height for the calibration curve as the peaks showed some tailing which made the AUC slightly inaccurate.

The SA concentration decreased seemingly linearly as shown in figure 27. The ASA curve seemed to show a plateau reached near a concentration of 0.045 mg/mL.

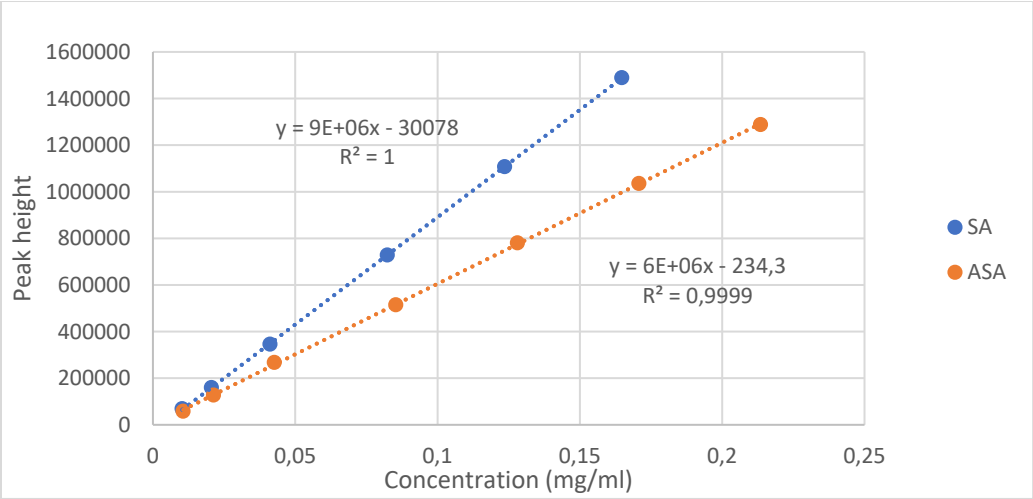

Figure 26: Typical example of the calibration curves measured during this study with peak height on the y-axis and the concentration in mg/mL on the x-axis. The SA curve is shown in blue and the ASA curve is shown in orange.

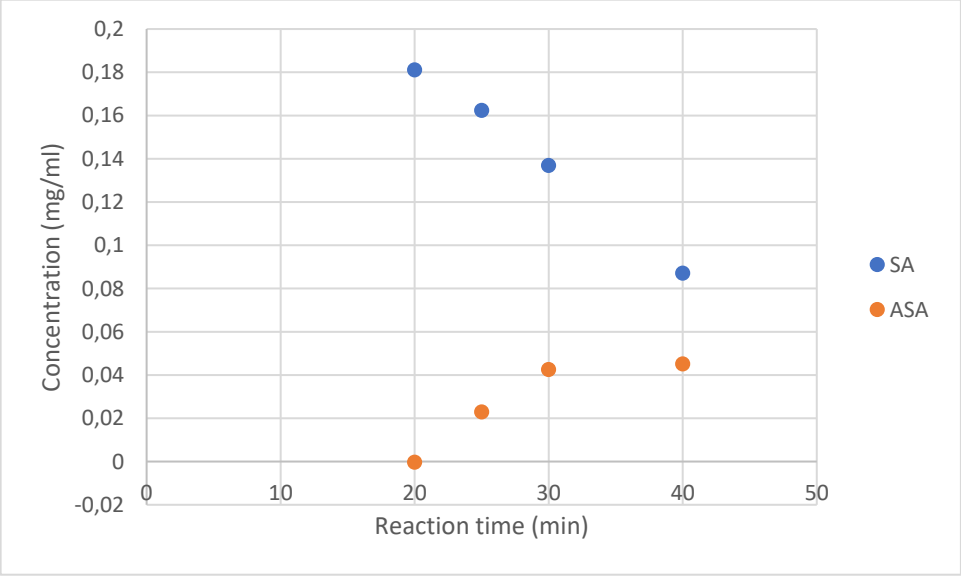

Figure 27: Graphical presentation of the concentration (mg/mL) of SA and ASA on the y-axis and the reaction time on the x-axis. Based on figure S13 and S14. Presenting the first results obtained with prototype 3.

The next day, reaction times of 50, 60 and 90 min were measured. The resulting graph in figure 28 shows that the linear decrease of SA concentration ends after a reaction time of 50 min. With a reaction time of 50 min, a higher ASA concentration was reached than the SA concentration. This was the minimal reaction time for a conversion of 50% or more. For the longer reaction times tested, the ASA concentration stayed higher than the SA concentration. The observed plateau after the first day was not continued with these new measurements. As they were measured on a different day and the set-up had to be built every day, it cannot be concluded if the measurement at 40 min was erroneous or if something was slightly different the next day that made higher conversion possible. It appears that the ASA concentration does not increase consistently as the reaction time increases, because a higher concentration was measured at 60 min than at 90 min reaction time. This might be explained by the small volume of only 1 µL of product pipetted making it prone to dilution errors. Possibly, a small droplet had attached to the outside of the pipet tip and more volume was added by accident.

The longest reaction times of 120 and 180 min were recorded on another day. For 120 min, figure 28 shows a significant increase in ASA concentration from circa 0.086 to 0.146 whereas the SA

concentration did not decrease much compared to the 90 min values. The 180 min reaction showed that almost all SA had reacted. However, the ASA concentration had decreased to circa 0.112 mg/mL. This was only slightly higher than the concentration measured for 60 min reaction time of 0.107 mg/mL.

The theoretical concentration of SA, based on 100% of the starting material, was around 0.138 mg/mL. The theoretical concentration of ASA, based on 100% conversion, was around 0.179 mg/mL. It is remarkable to see that for the shorter reaction times the calculated SA concentration exceeded this value. This could be due pipetting errors as described above or due to the fact that the concentrations measured were outside of the range used for the calibration curve. The concentrations used for the calibration curve were corrected after this.

It was difficult to draw conclusions from this graph as the measurements were obtained on different days and therefore slightly different systems. Also in this graph no plateau could be observed so no conclusions could be drawn about an optimal reaction time. For the practical reason of time limits, it was decided to use 180 min as optimal time. It was also decided to measure the reaction progression over time again later in a single system.

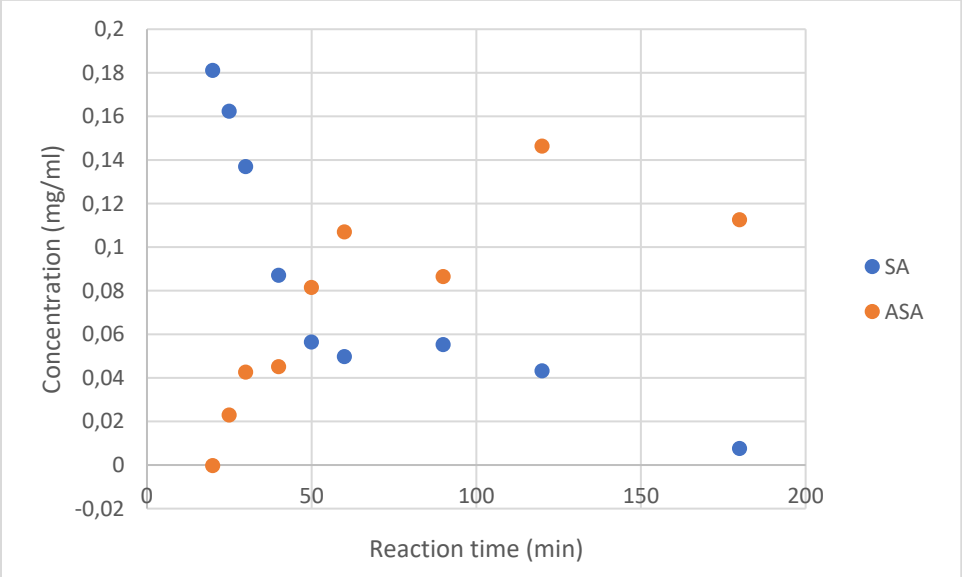

Figure 28: Graphical presentation of the concentration (mg/mL) of SA and ASA on the y-axis and the reaction time on the x-axis. Presenting the complete results obtained with prototype 3. Calculated using Figure S13, S14 for 20-40 min; figure S15, S16 for 50, 60 and 90 min; figure S23, S24 for 120 and 180 min.

To test the consistency of the system, the production of 180 min reaction time was monitored over 1 hour. Samples were taken 0, 15, 30, 45 and 60 min after product started to leave the system. In figure 31, the amounts of SA and ASA present are represented as percentages of the initial moles of SA in the system. In the sample taken directly after the system started producing around 5% of the starting amount of SA was present. However, only around 63% of the theoretical moles of ASA were formed, meaning around 30% of SA was converted into something else, possibly a side product of the reaction.

The chromatogram showed a peak of a compound being eluted around 0.6 min (figure 30). However, it is not very likely that this peak is a side product formed from SA as the short retention time indicates that the compound is very polar and it would not be expected for an organic compound to form such a polar compound. There are six common impurities to the synthesis reaction (figure 29): 4-hydroxybenzoic acid, 4-hydroxyisophthalic acid, salicylic acid, acetylsalicylic salicylic acid, salsalate

and acetylsalicylic anhydride (28). The five impurities other than salicylic acid have logP values of 1.6, 1.5, 3.8, 3.0 and 2.5 respectively (35–39). Most of them are relatively similar to either SA or ASA with the exception of acetylsalicylic salicylic acid. It is expected for this compound to have a longer retention time not shorter. None of these compounds would be able to cause the 0.6 min peak.

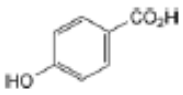

A. 4-hydroxybenzoic acid,

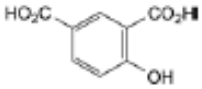

B. 4-hydroxybenzene-1,3-dicarboxylic acid (4-hydroxyisophthalic acid),

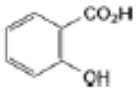

C. 2-hydroxybenzenecarboxylic acid (salicylic acid),

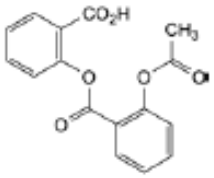

D. 2-[[2-(acetyloxy)benzoyl]oxy]benzoic acid (acetylsalicyl-salicylic acid),

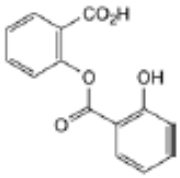

E. 2-[(2-hydroxybenzoyl)oxy]benzoic acid (salicylsalicylic acid),

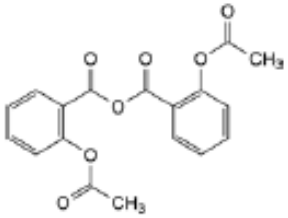

F. 2-(acetyloxy)benzoic anhydride (acetylsalicylic anhydride).

Figure 29: Molecular structures and systematic names of the six common impurities of Aspirin as stated by the European Pharmacopoeia (28).

Chromatograms for each separate reaction compound were measured (appendix 4.2). The acid catalysts H_3PO_4 and H_2SO_4 did not give a signal. Acetic acid gives a peak at 1.1 min, acetic anhydride at 2.2 min, EtOAc gives a signal at 3 min so it would most likely be covered by the ASA peak and ACN gives a peak at 1.4 min. The peaks at 1.1 min, 1.4 min and 2.2 min are explained by this. However, none of the known present compounds is responsible for the signal at 0.6 min. As the peak is relatively high and present in most of the chromatograms, it is not likely to be a incidental pollution, but rather a compound produced in or originating from the system. Other options were that chip material had ended up in the sample. This was deemed unlikely as the chips looked completely intact

when observed with a microscope after the reaction was performed. Also, PDMS is a hydrophobic polymer so it would be expected to stick to the column. Since the column had been washed thoroughly recently, it was unlikely that this was an unrelated compound being washed off the column. For the time being, this signal was left unidentified.

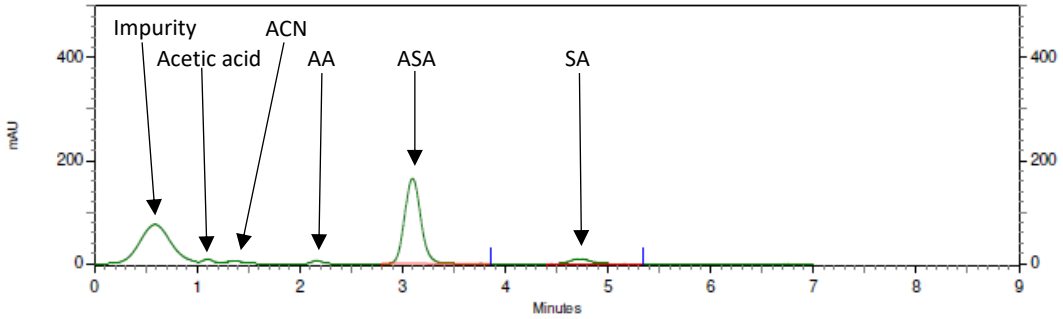

Figure 30: Chromatogram measured at 237 nm of the 180+0 measurement showing next to the ACN, ASA and SA peaks a strong signal at 0.6 min.

Figure 31 shows a slight increase of the ASA concentration to 67% in the samples taken after 15 and 30 min but went down to 53% for the two last measurements. After 45 min of production, SA was the major compound present again and after 60 min of production, the SA content was back to 75%. As nothing was changed during the measurements, it would be expected to see two fairly horizontal curves indicating a constant conversion and production of SA and ASA.

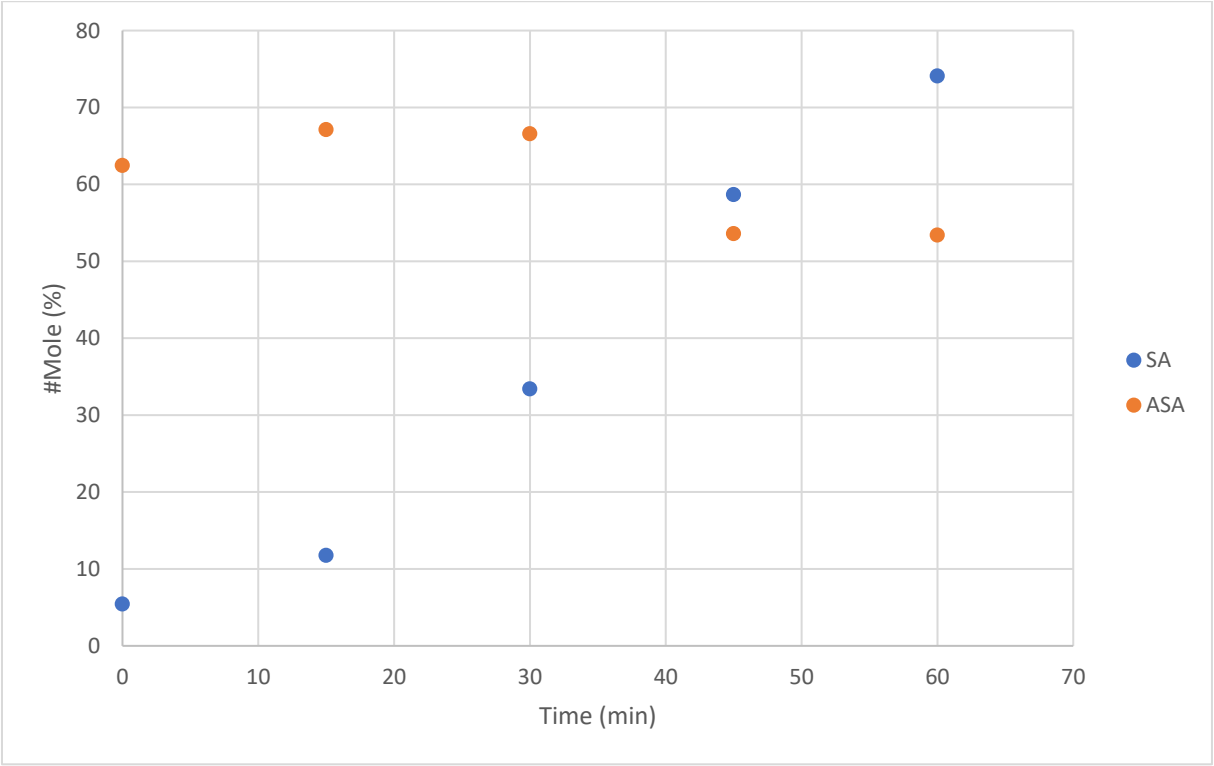

Figure 31: Graphical presentation showing the mole percentage of SA and ASA present compared to the initial moles of SA present in the system on the y-axis and the time the sample was taken after the system started producing on the x-axis. In blue SA and ASA in orange. Calculated with figure S17, S18.

The parafilm, wrapped around the glass syringe containing AA and H_3PO_4 for grip, had started to bunch up, indicating that this syringe had been slipping. During previous experiments, this did not

occur. This probably led to a lower AA to SA ratio causing the reaction to proceed slower as the equilibrium was pushed less towards the right. Another possibility was that the water in the phosphoric acid hydrolysed the AA to two acetic acid molecules. This would also effect the AA to SA ratio and therefore the reaction rate.

To prevent this from occurring the following adjustments were made. The compatibility of AA with a plastic syringe was tested and no interaction with the syringe and plunger material were observed. For AA, a plastic syringe was used in the following experiments. To eliminate the option of AA being degraded, the acid catalyst was added to the SA in EtOAc solution instead. Lastly, the acid catalyst was changed from 86% H_3PO_4 to 95% H_2SO_4. The rest of the concentrated acid solutions are water, so this was done to eliminate as much water as possible from the system.

3.4.4 Synthesis prototype 4

With one plastic syringe filled with pure AA (solution 1) and a glass syringe filled with SA in EtOAc with H_2SO_4 (solution 2) the previous experiment was repeated.

Figure 32 shows the expected horizontal curves for the mole percentages of SA and ASA present. SA is very consistently converted with only between 5.5 and 7% present for the different measurements. ASA was slightly less consistent with percentages between 75 and 85%. This variation was deemed acceptable as the measurements went up and down around 80% without sign of increase or decrease over time. The system was proven to be stable in its production of ASA.

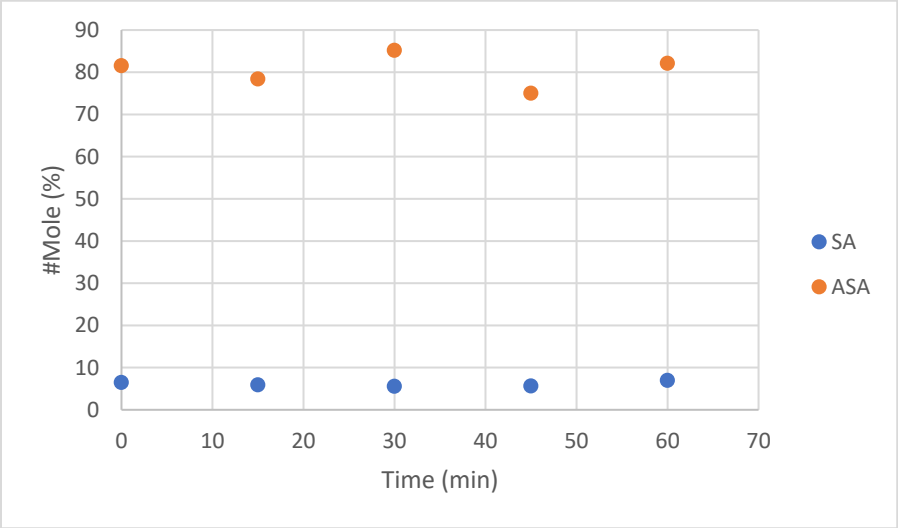

Figure 32: Graphical demonstration of the systems consistency by showing mole percentage of SA and ASA present compared to the initial moles of SA present in the system on the y-axis and the time the sample was taken after the system started producing on the x-axis. In blue SA and ASA in orange. Calculated with figure S19, S20.

3.4.5 Synthesis prototype 5

To obtain a good representation of the reaction progression over time, various reaction times were tested in a single system. This eliminated the effect of small inter-day variations. Figure 33 shows the incubation tubing used for this test.

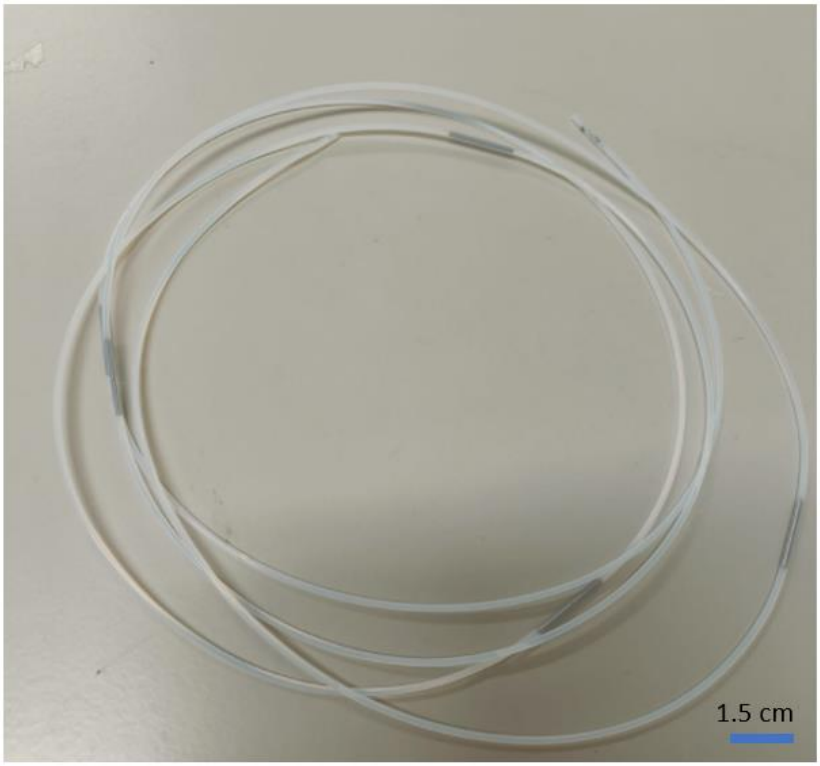

Figure 33: Incubation tubing divided into 30 cm segments representing 30 min reaction time and connected again by needles. Used to measure reaction progression in one system.

On the first attempt, it was observed that no product was being collected yet from the system at the expected time. In figure 34, a white solid can be seen around the plunger opening at the back of the syringe containing solution 2. There is also liquid visible between the plunger and syringe. This leakage could be due to small damage of the syringe or due to resistance from the system forcing the solution out through the back of the syringe. As the solution leaks out, the EtOAc evaporates and leaves SA behind. Examination of the reaction tubing showed many gas bubbles present in the latter part. Checking the nearby segment connection, the needle was found to have a sharp edge sticking out. It could be that this caused a small cut in the tubing that made it possible for air to enter the tubing or for the reaction mixture, especially EtOAc, to escape into the water bath.

All the tubing was replaced and new solutions were made for the second attempt. Figure 34 shows how this time SA could be seen as solid on the glass surrounding the chip. Analysing the chip closely showed that the inlet for solution 2 was leaking. This was not something that could be fixed.

Attempt 3 was conducted in the same manner as attempt 2, using a new chip. The same problem as for attempt 1 occurred with the syringe containing solution 2 leaking at the back. The most likely explanation was that the syringe had been damaged over the course of the experiments and started leaking because of it. A different explanation would be an increased resistance inside the system as the tubing was cut and reconnected with slightly narrower needles. However, even if this increased the resistance, the largest resistance in the system would still be the mixing structure at the start of the chip as the liquid is forced into the wells and up again breaking the otherwise smooth path. Therefore the effect of the needles would be negligible.

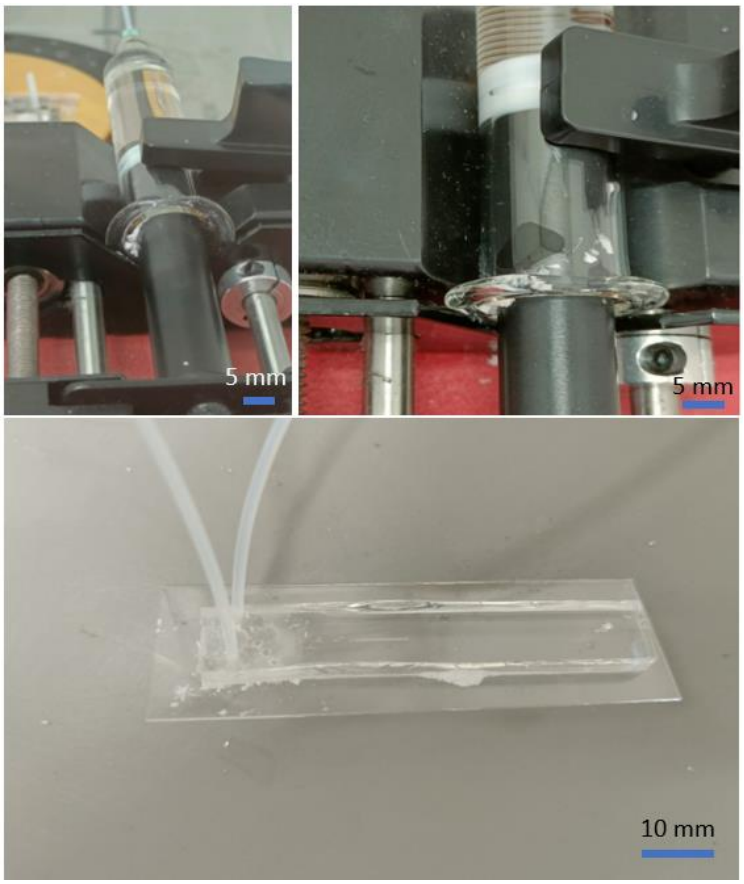

Figure 34: The top shows solid formed at the end of the syringe and liquid in between the plunger and the glass. The bottom shows solid formed around the chip due to leakage at the solution 2 inlet.

To increase the chances of success as much as possible, multiple improvements were made to the set-up. The syringe used for solution 2 was changed to a new 1-mL glass syringe. The reaction tubing was left intact with pen markings where each segment ended. The tubing was cut using a scalpel when taking the samples. The last change was the addition of a third syringe pump. The sharp needle and HPLC vial at the outlet were replaced by short tubing connected to a syringe in the third pump. This pump was set to withdraw at a rate of 5 µL/min. This means that even if the reaction mixture did not move forward properly through the system, this pump would aspirate the effluent at the intended rate.

3.4.6 Synthesis prototype 6

Figure 35 shows the last major changes to the set-up. The experiment was repeated and this time samples were collected for analysis. The reaction progression was measured at t=0, 30, 60, 90, 120, 150 and 180 min. In figure 36 the progression is graphically presented as the mole percentages of SA and ASA present at certain reaction times. The sample at t=0 was collected directly at the outlet of the chip and there already 10% of the SA was converted. The graph also shows that already 22% of the maximal moles of ASA were formed, indicating that there are some inaccuracies. This could be due to the previously explained pipetting and dilution errors. The general trend shows a steep decrease in SA for the reaction times of 30 and 60 min. Afterwards it seems to plateau around 2-3%. For ASA, a slightly less steep but consistent increase can be observed between reaction times of 0 to 90 min. After that, the formation goes up and down between 65 and 78%.

Based on these observations, 90 min seemed to be the optimal reaction time as no more significant increase in ASA was observed for the longer reaction times. It was decided to use a reaction time of

120 min for the final experiment to be sure that the maximal conversion had been reached in this system.

Figure 35: Addition of a third syringe pump connected to the end of the system set to withdraw at the same flowrate as the total flowrate into the system. A new syringe for solution 2 and a 10-mL syringe used for withdrawing.

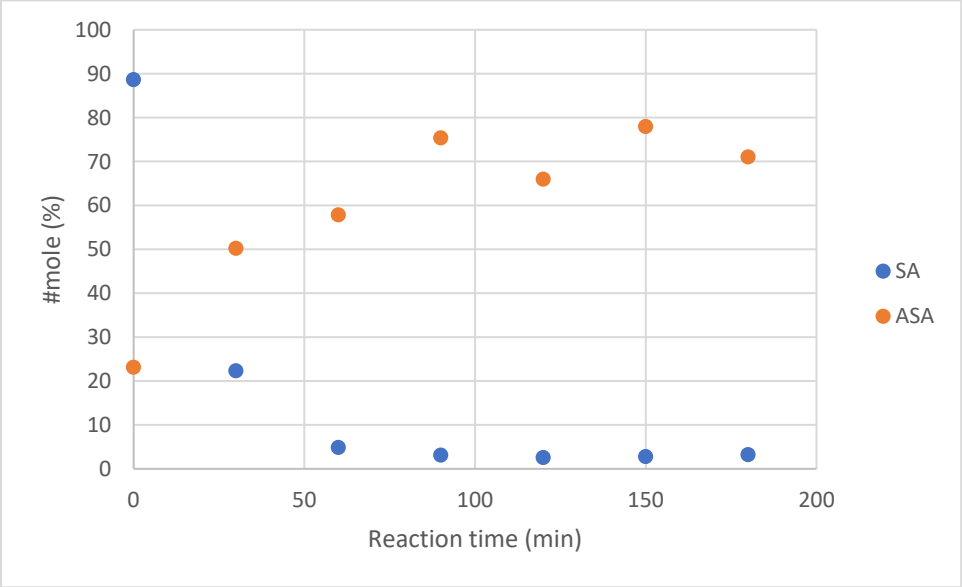

Figure 36: Graphical representation of the reaction progression with mole percentage on the y-axis and reaction time on the x-axis. Blue representing SA and orange for ASA. Calculated with figure 26.

4.3.7 synthesis prototype 7

The same set-up was used as for prototype 6 making use of the three syringe pumps. As this experiment was focussed on producing and collecting a larger amount of product for purification, a

higher flowrate was used that required longer tubing. Tubing of 359.7 cm and a total flowrate of 15 µL/min were used.

3.3165 g of product was collected at the end. The density of this solution was measured to be 0.947 g/mL by pipetting 1.0 mL of the product into a weighed vial and determining the mass. Based on this experimental density, 3.5021 mL had been collected. The theoretical yield would be 0.6293 g.

The product was stored in at -20 °C. At this temperature the EtOAc would remain a liquid whereas the rest would form a solid. A solid product of 0.79 g was obtained. Based on this mass and the theoretical yield, it could already be concluded that the product contained many impurities. After dissolving the product in EtOH an oil like substance was observed. The product did not readily recrystallise from the EtOH. This is often an indication that the product had a low purity. The obtained product had a mass of 0.4882 g. This translated to a yield of 78%. As only a relatively small amount of product was collected this yield was to expected. At every transfer step between glassware and the filtration set-up solid was left behind. The smaller the initial mass the larger this residue is in comparison.

The ASA content and purity were analysed using HPLC. Figure 37 shows that majority of the sample was ASA, but SA was still present. The calculated ASA concentration was 0.1966 mg/mL. Compared to the hypothetical concentration of 0.214 mg/mL this gave a ASA content of 92%. The calculated concentration of SA was 0.005066 mg/mL. This was around 2.4% of the total sample content. The ASA and SA content of the product do not add up to 100% so a few mass percent was not accounted for by the chromatogram. It is hypothesised that the remaining material would be water as it is difficult to completely dry the sample. This could be tested by heating the product to 105 °C for 15 min and weighing it to test for mass loss. A Karl-Fischer titration could also be used to determine the water content of the product (40). Observing the chromatogram of the purified product, it can be seen that this filtration and recrystallisation was successful in eliminating the unidentified impurity at 0.6 min. This was already expected as that compound was very polar and therefore likely to be soluble in water which was used in the recrystallisation.

The criteria for purified ASA as stated previously are a content of 99.5-100.5% and a SA content lower than 0.15% (28). The purified synthesis product met neither criteria.

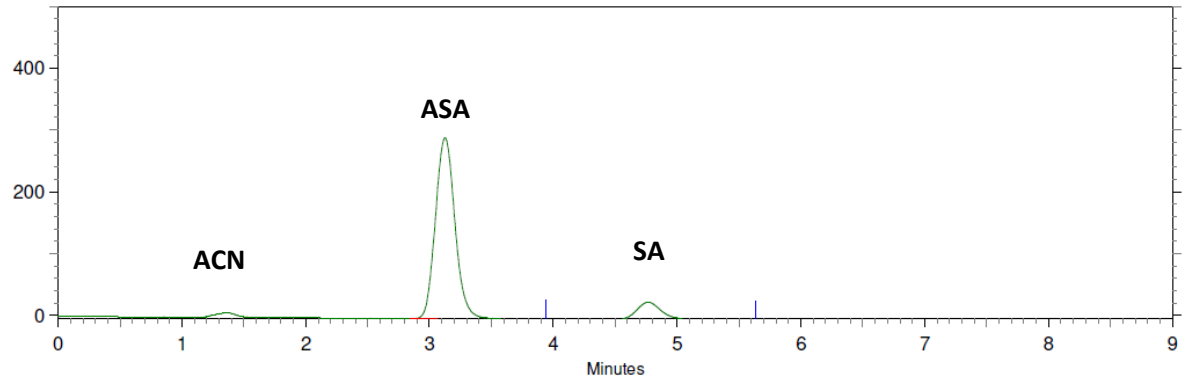

Figure 37: Chromatogram of the purified chip synthesis product showing a large peak for ASA at 3.2 min and a smaller peak for SA at 4.8 min.

4. Conclusion

The batch synthesis of aspirin from salicylic acid and acetic anhydride had a yield of 81%, a purity of 96-97% and an almost negligible amount of SA. The criteria for purified ASA as stated previously are a content of 99.5-100.5% and a SA content lower than 0.15% (28). The product did not meet the first criterion for aspirin. For the second criterion, this is not known as the SA amount was not quantified in the product. The chip system gave a reaction yield of around 80% and product yield of 78%. This purified product contained 92% aspirin, 2.4% salicylic acid and around 5% unidentified compounds. Majority of the 5% was hypothesised to be water as complete drying was difficult and no peaks of other compounds were observed in the chromatogram. This indicated that no other compounds were present with UV absorbance at the wavelength of 237 nm used for recording. Based on these values the ASA and SA content standards were not met.

The aim was to study if it was possible to synthesise aspirin on a microfluidic chip. The answer was found to be yes it is possible to perform aspirin synthesis on a microchip. As sub-question the efficiency of the system was compared to the batch synthesis considering the yield and purity. The yield was a little higher for the batch synthesis compared to the chip however not significantly. The purity of the batch synthesis product (96-97%) was higher than the purity of the chip product (92%). However, with one purification step neither product met the purity and ASA content criteria as stated by the European Pharmacopoeia.

4.2 Future outlook

Further research options would be testing more parameters to increase the yield of the reaction on the chip, such as different catalyst or reagent ratios as only around 80% of the expected amount of ASA was formed. In the case that this is the maximal conversion possible for this reaction and or system the focus would shift to optimisation of the purification. To create an effective purification method it would be important to know more about the impurities present. Mass spectroscopy is a good technique to analyse every compound present in a mix as it does not require absorption of light or radiation by a compound (20).

It would be of interest to design a second chip in the system connected directly to the first one where the purification would take place. A proposed mechanism is mixing the synthesis product with excess EtOH in a second staggered herringbone mixer chip and incubating it at 50 °C for a to be determined optimal time (30).

Further steps in making it a start-to-end flow system would be to develop a mechanism for continuous crystallisation and filtration. Examples include upscaling the production and connecting the system to a continuous flow tubular reactor and nucleator (41).

References

1. Kleinstreuer C. Modern Fluid Dynamics. 2nd ed. CRC Press; 2018.
2. Atencia J, Beebe DJ. Controlled microfluidic interfaces. Nature. 2005 Sep 28;437(7059):648–55.
3. Shashi Menon E. Transmission Pipeline Calculations and Simulations Manual. Gulf Professional Publishing; 2014.
4. Laminar Flow vs. Turbulent Flow [Internet]. Diffzi. 2018 [cited 2022 Mar 26]. Available from: https://diffzi.com/laminar-flow-vs-turbulent-flow/
5. Paul Mueller Company Engineering Staff. How does the reynolds number affect mixer design [Internet]. Paul Mueller Company Academy. 2018 [cited 2022 Mar 25]. Available from: https://nl.paulmueller.com/academy/how-does-the-reynolds-number-affect-mixer-design
6. Hunt B. Diffusion in laminar pipe flow. International Journal of Heat and Mass Transfer. 1977 Apr;20(4):393–401.
7. Ghorbani Kharaji Z, Kalantar V, Bayareh M. Acoustic sharp-edge-based micromixer: a numerical study. Chemical Papers. 2022 Mar 28;76(3):1721–38.
8. An Le NH, Deng H, Devendran C, Akhtar N, Ma X, Pouton C, et al. Ultrafast star-shaped acoustic micromixer for high throughput nanoparticle synthesis. Lab on a Chip. 2020;20(3):582–91.
9. Ajarostaghi SSM, Delavar MA, Poncet S. Thermal mixing, cooling and entropy generation in a micromixer with a porous zone by the lattice Boltzmann method. Journal of Thermal Analysis and Calorimetry. 2020 May 21;140(3):1321–39.
10. Du M, Ma Z, Ye X, Zhou Z. On-chip fast mixing by a rotary peristaltic micropump with a single structural layer. Sci China Technol. 2013;(56):1047–54.
11. Eickenberg B, Wittbracht F, Stohmann P, Schubert J-R, Brill C, Weddemann A, et al. Continuous-flow particle guiding based on dipolar coupled magnetic superstructures in rotating magnetic fields. Lab on a Chip. 2013;13(5):920.
12. Liu YZ, Kim BJ, Sung HJ. Two-fluid mixing in a microchannel. International Journal of Heat and Fluid Flow. 2004 Dec;25(6):986–95.
13. Su T, Cheng K, Wang J, Xu Z, Dai W. A fast design method for passive micromixer with angled bend. Microsystem Technologies. 2019 Nov 12;25(11):4391–7.
14. Hossain S, Kim K-Y. Parametric investigation on mixing in a micromixer with two-layer crossing channels. Springerplus. 2016 Dec 21;5(1):794.
15. Melin J, Giménez G, Roxhed N, Wijngaart W van der, Stemme G. A fast passive and planar liquid sample micromixer. Lab Chip. 2004;4(3):214–9.
16. Stroock AD, Dertinger SKW, Ajdari A, Mezić I, Stone HA, Whitesides GM. Chaotic Mixer for Microchannels. Science (1979). 2002 Jan 25;295(5555):647–51.

17. Dempsey DA, Klessig DF. How does the multifaceted plant hormone salicylic acid combat disease in plants and are similar mechanisms utilized in humans? BMC Biology. 2017 Dec 23;15(1):23.

18. Gala MK, Chan AT. Molecular Pathways: Aspirin and Wnt Signaling—A Molecularly Targeted Approach to Cancer Prevention and Treatment. Clinical Cancer Research. 2015 Apr 1;21(7):1543–8.

19. Altman R, Luciardi HL, Muntaner J, Herrera RN. The antithrombotic profile of aspirin. Aspirin resistance, or simply failure. Thrombosis Journal. 2004;2(1):1.

20. Mohrig J, Alberg D, Hofmeister G, Schatz P, Noring-Hammond C. Laboratory Techniques in Organic Chemistry. 4th ed. New York: W. H. Freeman and Company; 2014. 213–471 p.

21. Bhal SK. LogP—Making Sense of the Value. Advanced Chemistry Development. Toronto: ABClabs;

22. Graham C. Using Melting Point to Determine Purity of Crystalline Solids. In 2009.

23. Adamo A, Beingessner RL, Behnam M, Chen J, Jamison TF, Jensen KF, et al. On-demand continuous-flow production of pharmaceuticals in a compact, reconfigurable system. Science (1979). 2016 Apr 1;352(6281):61–7.

24. Sagandira CR, Siyawamwaya M, Watts P. 3D printing and continuous flow chemistry technology to advance pharmaceutical manufacturing in developing countries. Arabian Journal of Chemistry. 2020 Nov;13(11):7886–908.

25. Adamo A, Beingessner RL, Behnam M, Chen J, Jamison TF, Jensen KF, et al. On-demand continuous-flow production of pharmaceuticals in a compact, reconfigurable system. Science (1979). 2016 Apr 1;352(6281):61–7.

26. Microfluidics: A general overview of microfluidics. ElveFlow. 2022.

27. Niculescu A-G, Chircov C, Bîrcă AC, Grumezescu AM. Fabrication and Applications of Microfluidic Devices: A Review. International Journal of Molecular Sciences. 2021 Feb 18;22(4):2011.

28. Council of Europe. the European Pharmacopoeia. 10.0. Strasbourg: Council of Europe; 2019. 1753–1755 p.

29. Chemistry 104: Synthesis of Aspirin [Internet]. [cited 2022 Feb 14]. Available from: http://www.chem.latech.edu/~deddy/chem104/104Aspirin.htm

30. Balogh A, Domokos A, Farkas B, Farkas A, Rapi Z, Kiss D, et al. Continuous end-to-end production of solid drug dosage forms: Coupling flow synthesis and formulation by electrospinning. Chemical Engineering Journal. 2018 Oct;350:290–9.

31. What Causes Peak Tailing in HPLC. ChromTech Inc. 2021.

32. Petrino PJ, Gaston-Bonhomme YH, Chevalier JLE. Viscosity and Density of Binary Liquid Mixtures of Hydrocarbons, Esters, Ketones, and Normal Chloroalkanes. Journal of Chemical & Engineering Data. 1995 Jan 1;40(1):136–40.

33. PubChem Compound Summary for CID 8857, Ethyl acetate [Internet]. National Center for Biotechnology Information. 2022 [cited 2022 Mar 26]. Available from: https://pubchem.ncbi.nlm.nih.gov/compound/Ethyl-acetate

34. Barrera NIG, Bories C, Peydecastaing J, Sablayrolles C, Vedrenne E, Vaca-Garcia C, et al. A Novel Process Using Ion Exchange Resins for the Coproduction of Ethyl and Butyl Acetates. Green and Sustainable Chemistry. 2018;08(03):221–46.

35. PubChem Compound Summary for CID 135, 4-Hydroxybenzoic acid. National Center for Biotechnology Information . 2022.

36. PubChem Compound Summary for CID 12490, 4-Hydroxyisophthalic acid. National Center for Biotechnology Information. 2022.

37. PubChem Compound Summary for CID 129715664. National Center for Biotechnology Information. 2022.

38. PubChem Compound Summary for CID 5161, Salsalate. National Center for Biotechnology Information. 2022.

39. PubChem Compound Summary for CID 15110, Acetylsalicylic anhydride. National Center for Biotechnology Information. 2022.

40. Bozic D. What Is Karl Fischer Titration and What Are Its Applications? [Internet]. AZO Materials. 2018 [cited 2022 Apr 6]. Available from: https://www.azom.com/article.aspx?ArticleID=16017

41. Rimez B, Septavaux J, Scheid B. The coupling of in-flow reaction with continuous flow seedless tubular crystallization. Reaction Chemistry & Engineering. 2019;4(3):516–22.

42. OpenStax CNX. 14.5 Fluid Dynamics [Internet]. University Physics OpenStax. [cited 2022 Mar 26]. Available from: https://courses.lumenlearning.com/suny-osuniversityphysics/chapter/14-5-fluid-dynamics/

Appendices

Appendix 1: Calculation of Reynolds numbers

Calculated for the designed system in section 2.3.

Assumptions:

- Circular channels with 300 µm diameter
- Only the viscosity of the main component ethyl acetate (at 50 °C)
- For the most used flowrate of 5 µl/min

Flow velocity: $Q = A * V$; with Q being the flow rate in L/s, A the cross-sectional area of the channel in m^2 and V the flow velocity in m/s (42).

⇨ $V = \frac{Q}{A} = \frac{(8.3*10^{-8})*10^{-3}}{(150*10^{-6})^2*\pi} = 1.169 * 10^{-3}\ m/s$

Reynolds number: $R = \frac{V*L}{v}$; with V being the flow velocity in m/s, L the diameter of the channel in m and v the kinematic viscosity of the solution in m^2/s.

$R = \frac{(1.169*10^{-3})*(300*10^{-6})}{(3.8199*10^{-7})} = 0.92$

Appendix 2: Batch synthesis

Appendix 2.1 HLPC

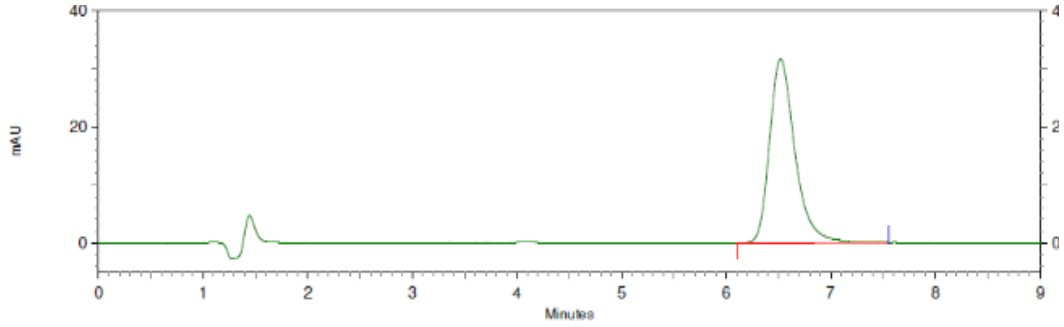

DAD-CH1 237 nm Results

Retention Time	Area	Height
6.520	2151984	126766
Totals	2151984	126766

Figure S1: Chromatogram of only SA in ACN. 17 February 2022

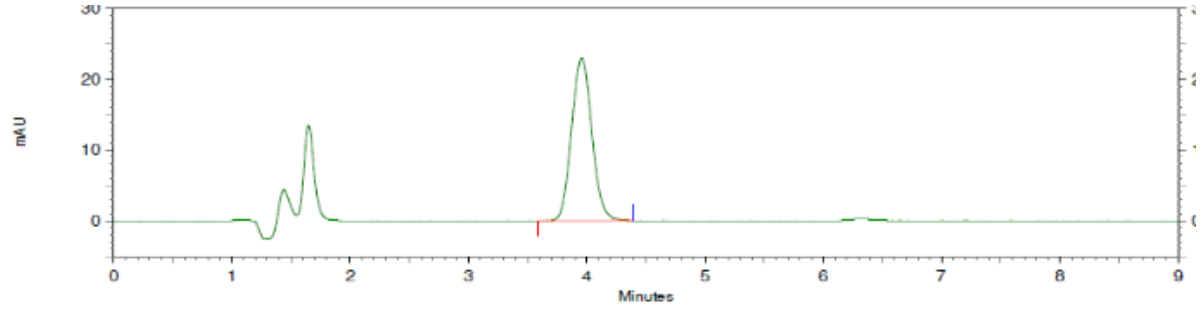

DAD-CH1 237 nm Results

Retention Time	Area	Height
3.960	1097902	91663
Totals	1097902	91663

Figure S1: Chromatogram of only ASA in ACN 17 February 2022

Eluent testing

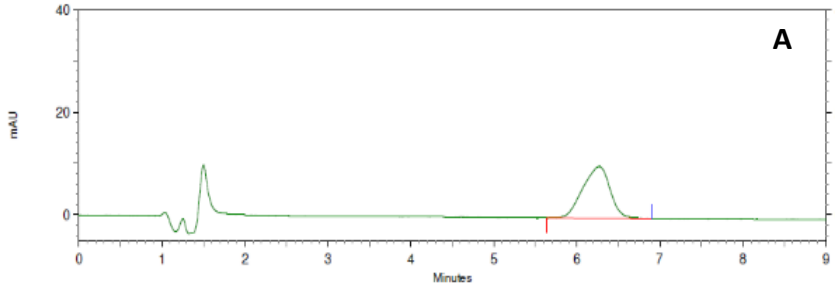

DAD-CH1 237 nm Results

Retention Time	Area	Height
6.267	922618	40296
10.427	1680484	56146
Totals	2603102	96442

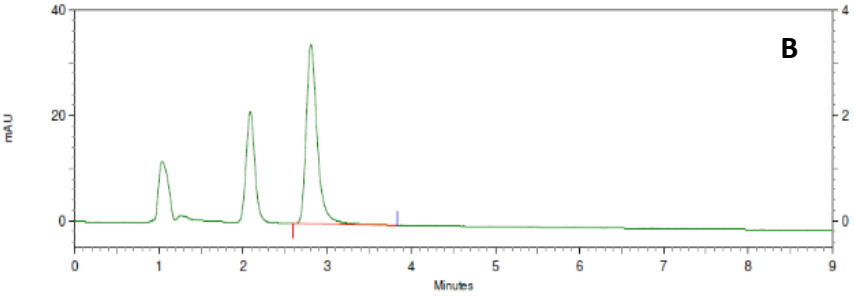

DAD-CH1 237 nm Results

Retention Time	Area	Height
2.807	1246915	136065
Totals	1246915	136065

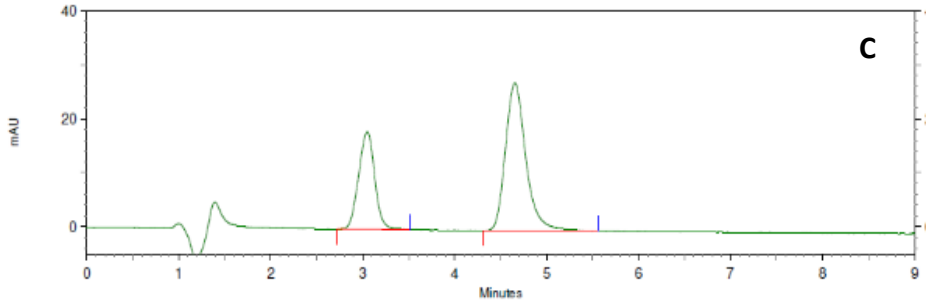

DAD-CH1 237 nm Results

Retention Time	Area	Height
3.053	877389	72140
4.653	1690574	109485
Totals	2567963	181625

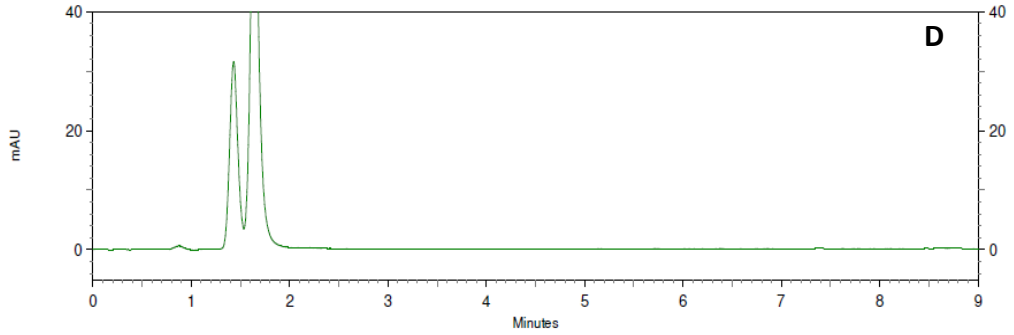

DAD-CH1 237 nm Results

Retention Time	Area	Height

Figure S2: the chromatograms presenting the separation of SA and ASA on a RP-HPLC using various ratios of UP water with H_3PO_4 to ACN. A: 80:20 UP water to ACN; B: 60:40 UP water to ACN; C: 70:30 UP water to ACN; D: 40:60 UP water to ACN. Measured 17 February 2022

Calibration curve 21-2-2022

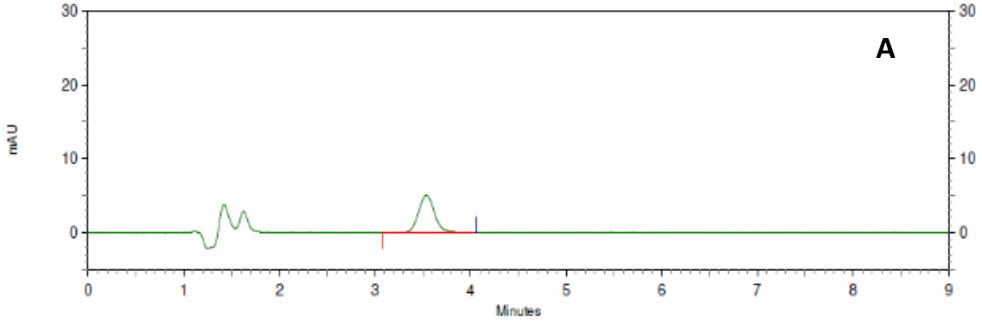

DAD-CH1 237 nm Results

Retention Time	Area	Height
3.533	237906	20210
Totals	237906	20210

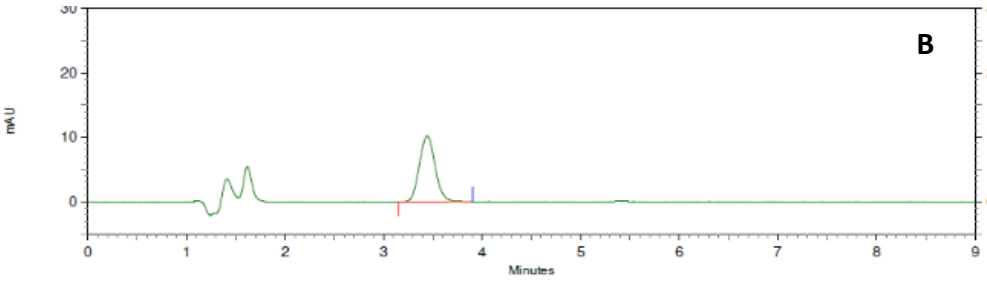

DAD-CH1 237 nm Results

Retention Time	Area	Height
3.440	452779	40757
Totals	452779	40757

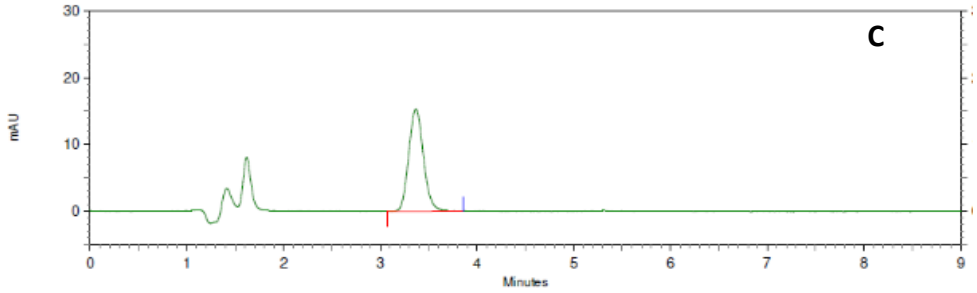

DAD-CH1 237 nm Results

Retention Time	Area	Height
3.367	650711	61221
Totals		
	650711	61221

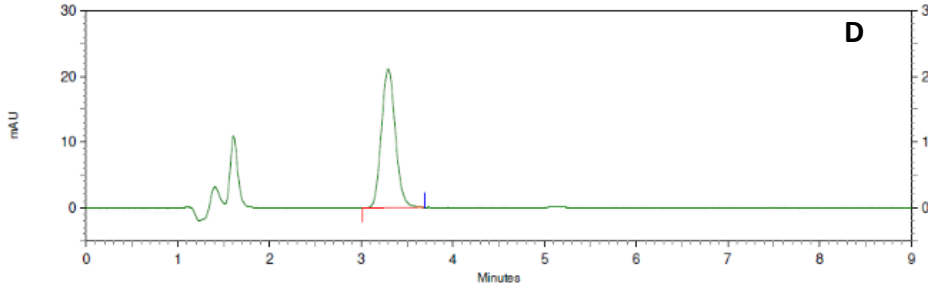

DAD-CH1 237 nm Results

Retention Time	Area	Height
3.293	895791	84408
Totals		
	895791	84408

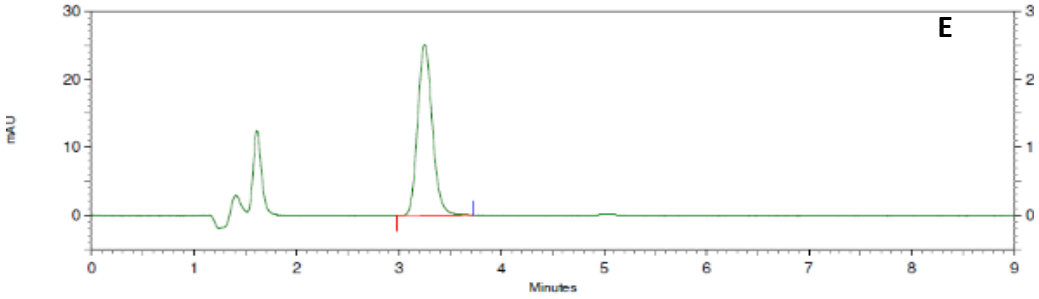

DAD-CH1 237 nm Results

Retention Time	Area	Height
3.253	1001959	100550
Totals		
	1001959	100550

Figure S3: Chromatographs measured on 21-2-2022 for the ASA calibration curve . A: sample concentration of 0.00396; B: sample concentration of 0.00792; C: sample concentration of 0.01188; D: sample concentration of 0.01584; :sample concentration of 0.0198.

Calculations:

Trendline equation: Y=5*10^7x+56494

Sample concentration: 1113081=5*10^7x+56494

X=0.0211 mg/mL

Purity 0.0218/0.0211 *100%= 97%

Appendix 2.2 IR Spectra

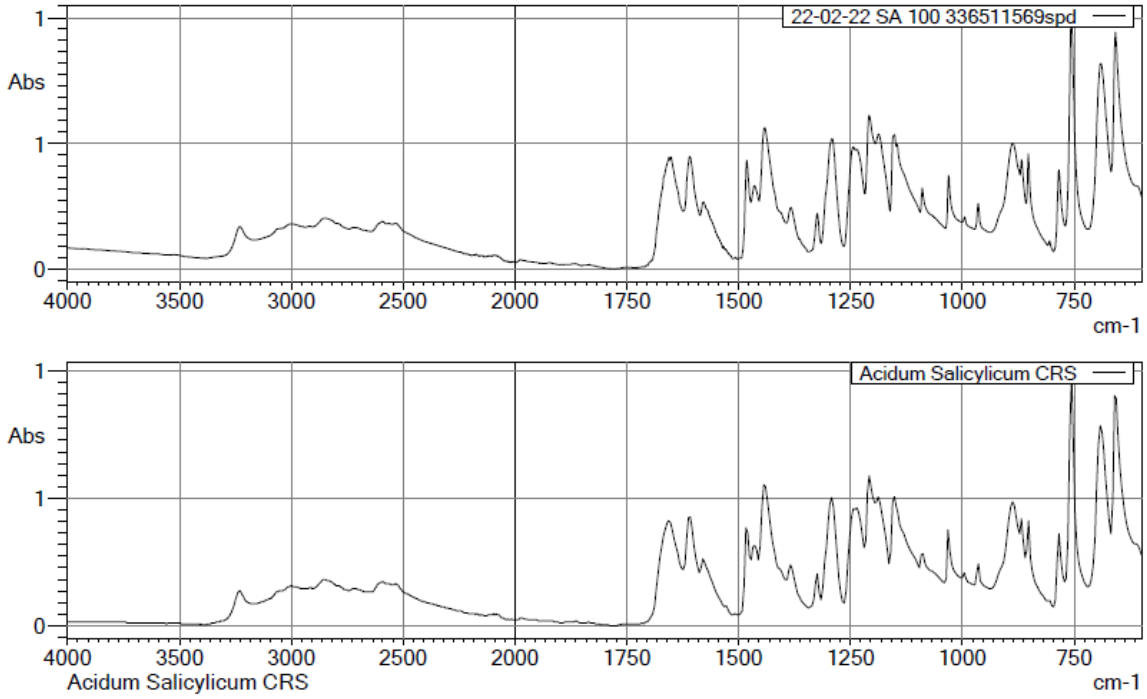

C:¥LabSolutions¥LabSolutionsIR¥Data¥22-02-22 SA 100 336511569spd.ispd

	Score	Library	Name	Comment
1	992	15 - RUG	Acidum Salicylicum CRS	Acidum Salicylicum CRS
2	962	76 - Pharmaceutische grondstoffen Leverancier BUFA	ACIDUM SALICYLICUM (90) - PH.EUR. - BUFA - 97D16FR	ACIDUM SALICYLICUM (90) - PH.EUR. - BUFA - 97D16FR
3	962	400 - Pharmaceutische grondstoffen Leverancier BUFA	ACIDUM SALICYLICUM (90) - PH.EUR. - BUFA - 97D16FR	ACIDUM SALICYLICUM (90) - PH.EUR. - BUFA - 97D16FR
4	962	79 - Pharmaceutische grondstoffen Leverancier BUFA	ACIDUM SALICYLICUM (90) - PH.EUR. - BUFA - 97D16FR	ACIDUM SALICYLICUM (90) - PH.EUR. - BUFA - 97D16FR
5	961	69 - Pharmaceutische grondstoffen Leverancier BUFA	ACIDUM SALICYLICUM (180) - PH.EUR. - BUFA - 97D11FR	ACIDUM SALICYLICUM (180) - PH.EUR. - BUFA - 97D11FR

Figure S4: IR spectrum of 100% SA and 0% ASA with the best matches in literature as determined by the software.

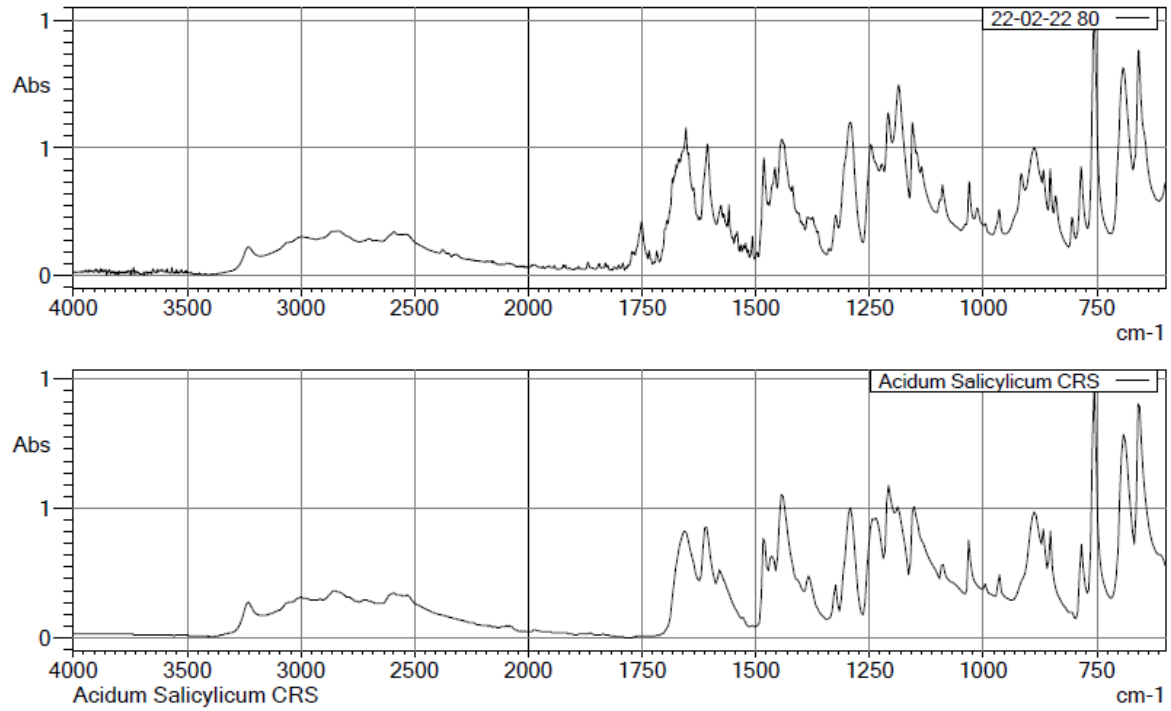

C:¥LabSolutions¥LabSolutionsIR¥Data¥22-02-22 80.ispd

	Score	Library	Name	Comment
1	970	15 - RUG	Acidum Salicylicum CRS	Acidum Salicylicum CRS
2	937	76 - Pharmaceutische grondstoffen Leverancier BUFA	ACIDUM SALICYLICUM (90) - PH.EUR. - BUFA - 97D16FR	ACIDUM SALICYLICUM (90) - PH.EUR. - BUFA - 97D16FR
3	937	400 - Pharmaceutische grondstoffen Leverancier BUFA	ACIDUM SALICYLICUM (90) - PH.EUR. - BUFA - 97D16FR	ACIDUM SALICYLICUM (90) - PH.EUR. - BUFA - 97D16FR
4	937	79 - Pharmaceutische grondstoffen Leverancier BUFA	ACIDUM SALICYLICUM (90) - PH.EUR. - BUFA - 97D16FR	ACIDUM SALICYLICUM (90) - PH.EUR. - BUFA - 97D16FR
5	934	69 - Pharmaceutische grondstoffen Leverancier BUFA	ACIDUM SALICYLICUM (180) - PH.EUR. - BUFA - 97D11FR	ACIDUM SALICYLICUM (180) - PH.EUR. - BUFA - 97D11FR

Figure S5: IR spectrum of 80% SA and 20% ASA with the best matches in literature as determined by the software.

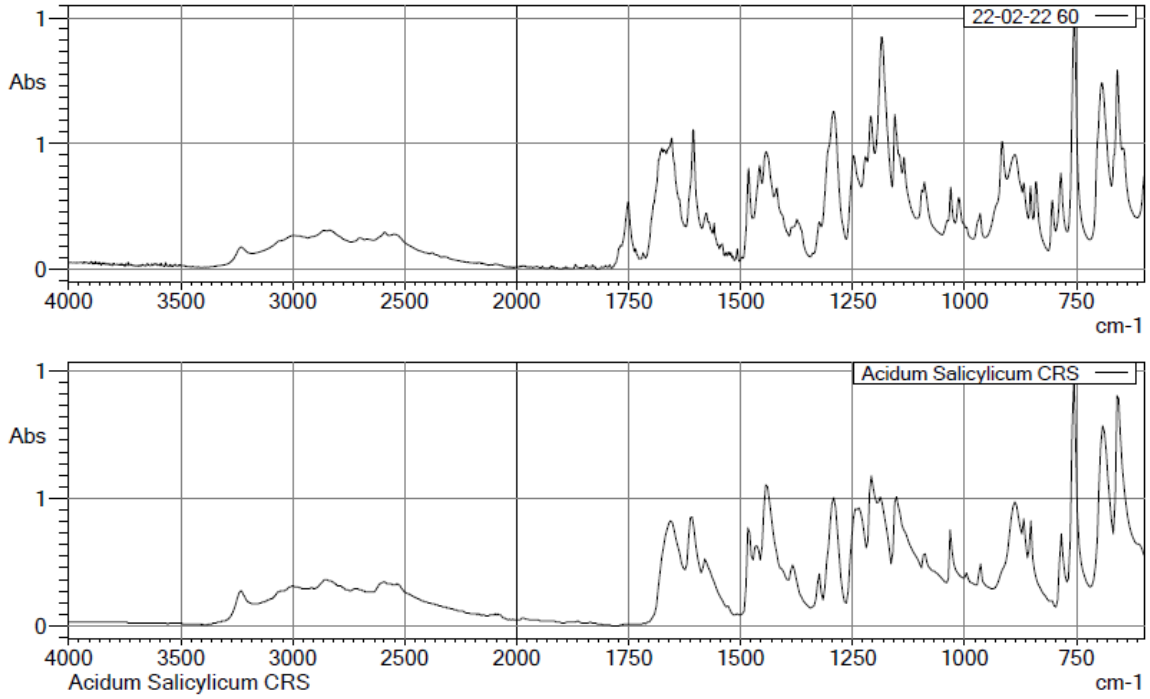

C:¥LabSolutions¥LabSolutionsIR¥Data¥22-02-22 60.ispd

	Score	Library	Name	Comment
1	925	15 - RUG	Acidum Salicylicum CRS	Acidum Salicylicum CRS
2	887	76 - Pharmaceutische grondstoffen Leverancier BUFA	ACIDUM SALICYLICUM (90) - PH.EUR. - BUFA - 97D16FR	ACIDUM SALICYLICUM (90) - PH.EUR. - BUFA - 97D16FR
3	887	400 - Pharmaceutische grondstoffen Leverancier BUFA	ACIDUM SALICYLICUM (90) - PH.EUR. - BUFA - 97D16FR	ACIDUM SALICYLICUM (90) - PH.EUR. - BUFA - 97D16FR
4	887	79 - Pharmaceutische grondstoffen Leverancier BUFA	ACIDUM SALICYLICUM (90) - PH.EUR. - BUFA - 97D16FR	ACIDUM SALICYLICUM (90) - PH.EUR. - BUFA - 97D16FR
5	885	69 - Pharmaceutische grondstoffen Leverancier BUFA	ACIDUM SALICYLICUM (180) - PH.EUR. - BUFA - 97D11FR	ACIDUM SALICYLICUM (180) - PH.EUR. - BUFA - 97D11FR

Figure S6: IR spectrum of 60% SA and 40% ASA with the best matches in literature as determined by the software.

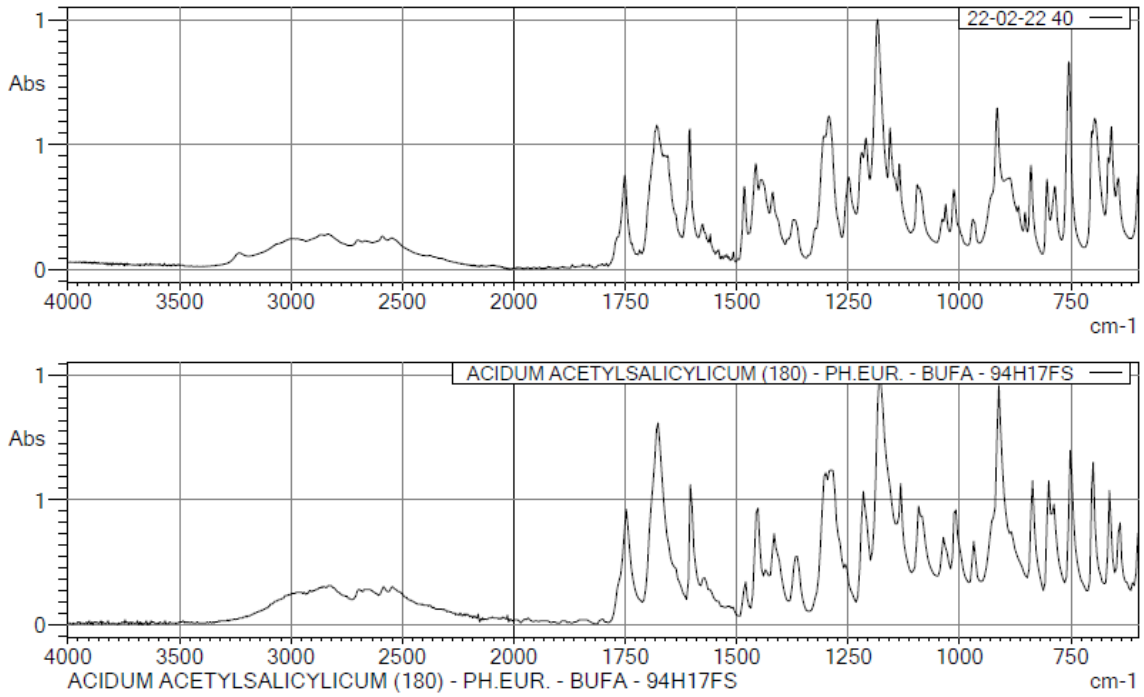

C:¥LabSolutions¥LabSolutionsIR¥Data¥22-02-22 40.ispd

	Score	Library	Name	Comment
1	894	140 - Pharmaceutische grondstoffen Leverancier BUFA	ACIDUM ACETYLSALICYLICUM (180) - PH.EUR. - BUFA - 94H17FS	ACIDUM ACETYLSALICYLICUM (180) - PH.EUR. - BUFA - 94H17FS
2	894	465 - Pharmaceutische grondstoffen Leverancier BUFA	ACIDUM ACETYLSALICYLICUM (180) - PH.EUR. - BUFA - 94H17FS	ACIDUM ACETYLSALICYLICUM (180) - PH.EUR. - BUFA - 94H17FS
3	894	144 - Pharmaceutische grondstoffen Leverancier BUFA	ACIDUM ACETYLSALICYLICUM (180) - PH.EUR. - BUFA - 94H17FS	ACIDUM ACETYLSALICYLICUM (180) - PH.EUR. - BUFA - 94H17FS
4	818	15 - RUG	Acidum Salicylicum CRS	Acidum Salicylicum CRS

Figure S7: IR spectrum of 40% SA and 60% ASA with the best matches in literature as determined by the software.

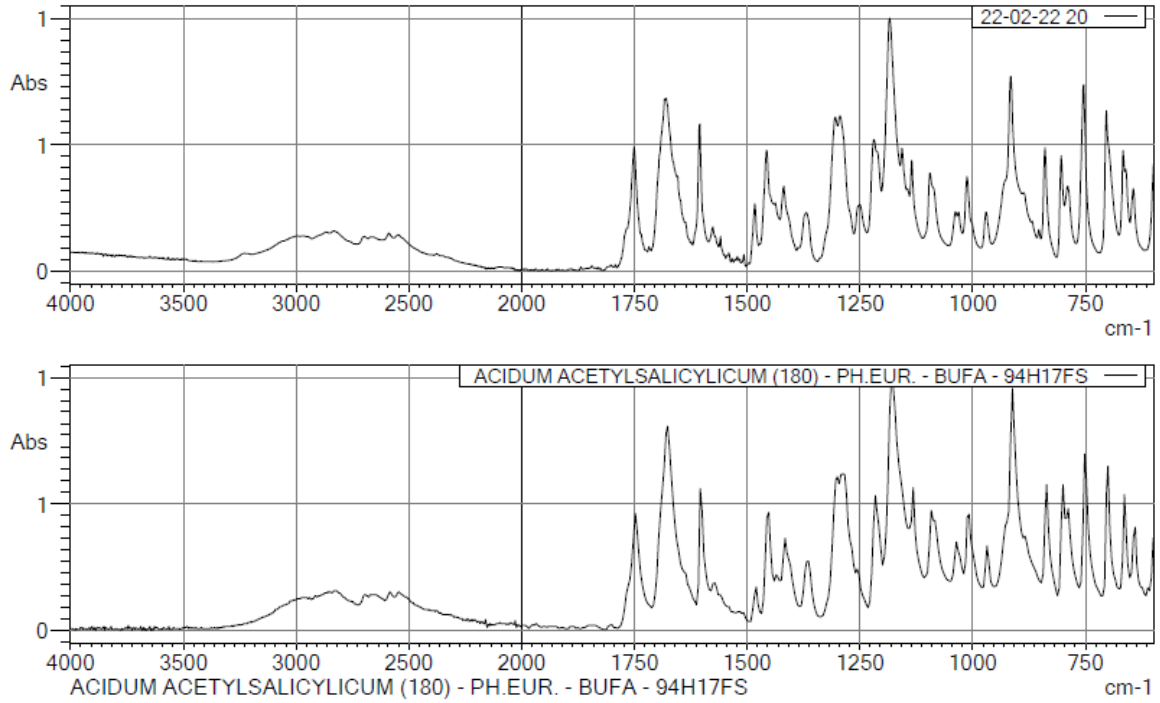

C:¥LabSolutions¥LabSolutionsIR¥Data¥22-02-22 20.ispd

	Score	Library	Name	Comment
1	903	140 - Pharmaceutische grondstoffen Leverancier BUFA	ACIDUM ACETYLSALICYLICUM (180) - PH.EUR. - BUFA - 94H17FS	ACIDUM ACETYLSALICYLICUM (180) - PH.EUR. - BUFA - 94H17FS
2	903	465 - Pharmaceutische grondstoffen Leverancier BUFA	ACIDUM ACETYLSALICYLICUM (180) - PH.EUR. - BUFA - 94H17FS	ACIDUM ACETYLSALICYLICUM (180) - PH.EUR. - BUFA - 94H17FS
3	903	144 - Pharmaceutische grondstoffen Leverancier BUFA	ACIDUM ACETYLSALICYLICUM (180) - PH.EUR. - BUFA - 94H17FS	ACIDUM ACETYLSALICYLICUM (180) - PH.EUR. - BUFA - 94H17FS

Figure S8: IR spectrum of 20% SA and 80% ASA with the best matches in literature as determined by the software.

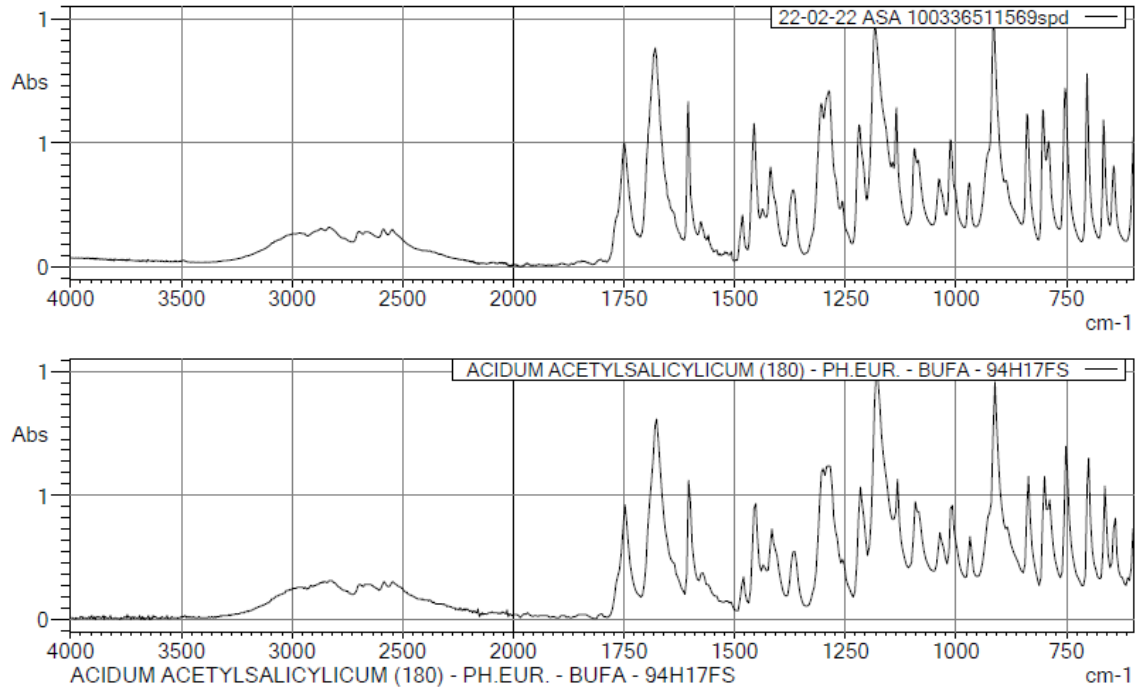

C:¥LabSolutions¥LabSolutionsIR¥Data¥22-02-22 ASA 100336511569spd.ispd

	Score	Library	Name	Comment
1	957	140 - Pharmaceutische grondstoffen Leverancier BUFA	ACIDUM ACETYLSALICYLICUM (180) - PH.EUR. - BUFA - 94H17FS	ACIDUM ACETYLSALICYLICUM (180) - PH.EUR. - BUFA - 94H17FS
2	957	465 - Pharmaceutische grondstoffen Leverancier BUFA	ACIDUM ACETYLSALICYLICUM (180) - PH.EUR. - BUFA - 94H17FS	ACIDUM ACETYLSALICYLICUM (180) - PH.EUR. - BUFA - 94H17FS
3	957	144 - Pharmaceutische grondstoffen Leverancier BUFA	ACIDUM ACETYLSALICYLICUM (180) - PH.EUR. - BUFA - 94H17FS	ACIDUM ACETYLSALICYLICUM (180) - PH.EUR. - BUFA - 94H17FS

Figure S9: IR spectrum of 0% SA and 100% ASA with the best matches in literature as determined by the software.

Appendix 3: Clean Room protocols

Procedure with photoresist SU-8 2-layer [**60 & 50 μm structures**]

Layer of SU-8 2025 of 60 μm thick for channel structures.
One layer SU-8 2025 with structures of 50 micron high for herringbone grooves
Author: Pim, June 4th, 2018

Wafer cleaning
* Rinse wafer once with acetone.
* Rinse wafer once with isopropanol.
* Rinse wafer once with milliQ; centrifuge it dry.
* Heat wafer for 30 minutes at 150ºC [hot plate]; cool down.

1ST LAYER – 60 μm
Spincoat step with CEE™ –100 spincoater
* Center the wafer on **small chuck** of the spincoater by using the spincoat program; start it; press on 0 till the wafer is centred.
* Add slowly *4 mL SU-8 2025* on the middle of the wafer; avoid air-bubbles.
* Use the spincoat program:
[0] Velocity: 500 rpm
[0] Ramp: 100 rpm/s
[0] Time: 10 s
[1] Velocity: **1450** rpm
[1] Ramp: 300 rpm/s
[1] Time: **30** s

Soft bake step
* Set the two hotplates in the wet bench to 65 and 95°C in advance; cover with inverted Petri dishes
* Heat the wafer for **3** min at 65º C.
* Heat the wafer for **7** min at 95º C.
* Remove the wafer from the hotplate to cool it to room temperature on a tissue.

Exposure step; OAI UV exposure system (365 nm) with mask 1
* Switch on the UV-lamp and heat the lamp for 10 min.
* Measure output of the lamp [~10 mW/cm^2] with glass plate.
* Put the wafer + mask 1 + glass plate under the lamp
* Expose the wafer with 235 mJ/cm^2 (~22 sec).

Post exposure bake
* Put the wafer on the hot-plate. Cover aluminum wafer dishes with inverted Petri dishes.
* Heat the wafer **2** min at 65º C.
* Heat the wafer **6** min at 95º C.

Activation of SU-8 layer
* Oxygen plasma treatment: 310-320 mTorr for 20” [outside the cleanroom]

2ND LAYER – 50 µm

Spincoat step with CEE™ –100 spincoater

* Center the wafer on the small chuck of the spincoater by using the spincoat program 1; start it; press on 0 till the wafer is centered.
* Add slowly 4 mL SU-8 2025 on the middle of the wafer; avoid air-bubbles.
* Use the spincoat program 1:

[0] Velocity: 500 rpm
[0] Ramp: 100 rpm/s
[0] Time: 10 s
[1] Velocity: **1730** rpm
[1] Ramp: 300 rpm/s
[1] Time: **30** s

Soft bake step

* Set the two hotplates in the wet bench to 65 and 95°C in advance; cover with inverted Petri dishes
* Heat the wafer for **3** min at 65° C.
* Heat the wafer for **6** min at 95° C.
* Remove the wafer from the hotplate to cool it to room temperature on a tissue.

Exposure step; OAI UV exposure system (365 nm) with mask 2

* Switch on the UV-lamp and heat the lamp for 10 min.
* Measure output of the lamp [~10 mW/cm^2] with glass plate.
* Align mask 2 on wafer
* Put the wafer + mask 2 + glass plate under the lamp
* Expose the wafer with 207 mJ/cm^2 (~20 sec).

Post exposure bake

* Put the wafer on the hot-plate. Cover aluminum wafer dishes with inverted Petri dishes.
* Heat the wafer **2** min at 65° C.
* Heat the wafer **6** min at 95° C.

Development

* Put the wafer in a glass Petri-dish with SU-8 developer.
* Move the wafer from time to time till all non-exposed SU-8 is solved [2 minutes].
* *Mini-shaker conditions*: orbital 60; 15 sec; reciprocal 360°; 0 sec; vibro 5°; 2 sec; cycle 100
* Develop another 8 minutes with fresh developer.
* Check if the development is completed by rinsing with isopropanol.
* If there is non-exposed SU-8 on the wafer, the wafer or parts of the wafer will be white; incubate it in SU-8 developer.
* If all non-exposed SU-8 is removed then dry it and put it in a Petri-dish.

Extra steps:

Hardbake step

***** To make structures stronger and repair cracks.
* Put the master on the hotplate at 150° C and incubate for 20 min.
* Cool down passively till 65° C.

Silanization

* To remove PDMS more easily for the SU-8 masters.
* Incubate the master with 10 μL TCOPS for 30 minutes under vacuum [in a desiccator].

Appendix 4: HPLC Data Chip Synthesis

Appendix 4.1: Calibration curves

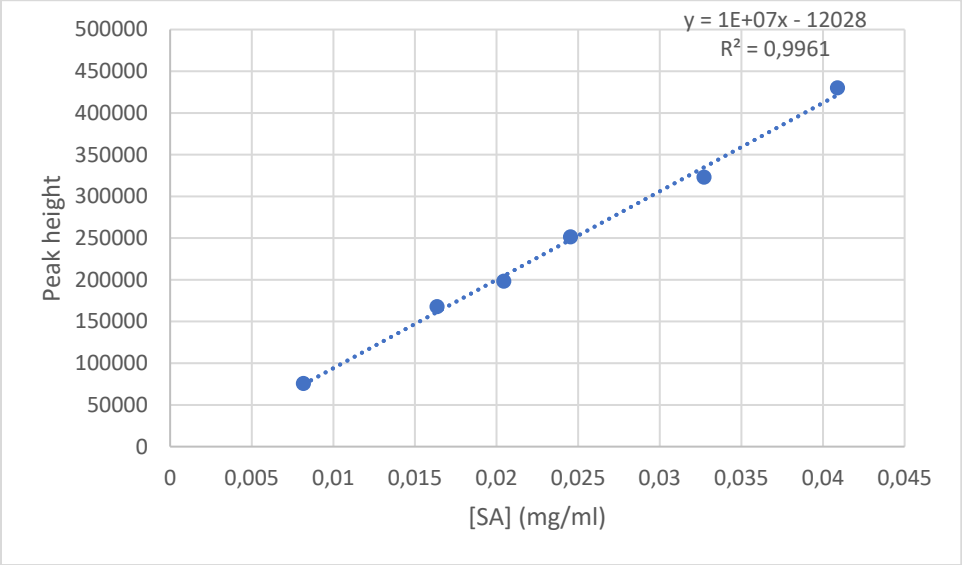

Figure S10: Calibration curve for SA with peak height on the y-axis against concentration on the x-axis. Measured on 2 March 2022

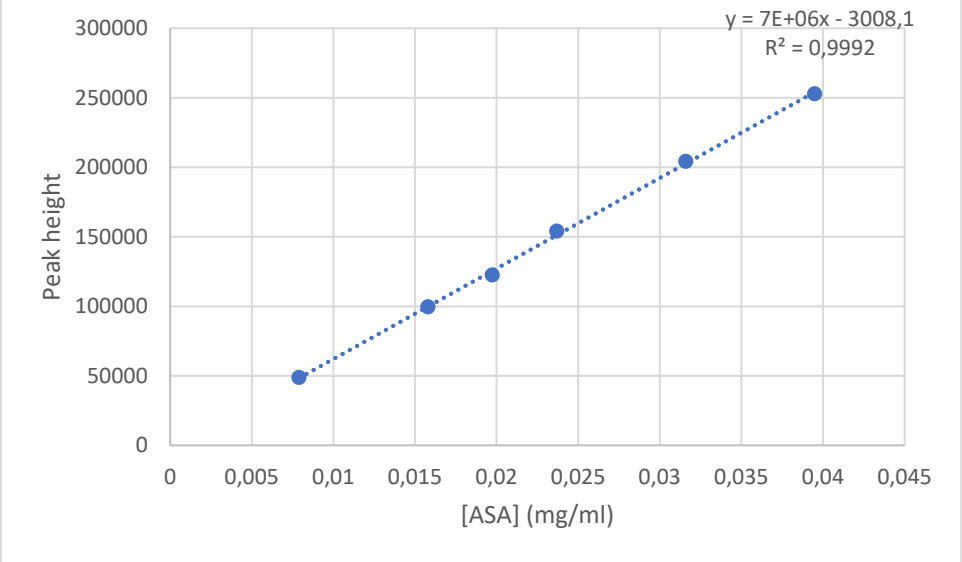

Figure S11: Calibration curve for ASA with peak height on the y-axis against concentration on the x-axis. Measured on 2 March 2022

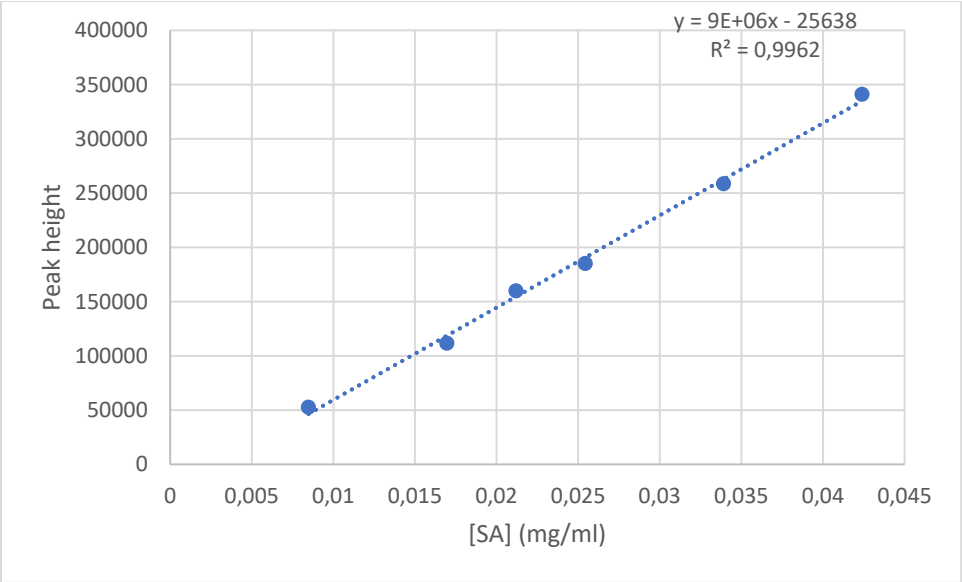

Figure S12: Calibration curve for SA with peak height on the y-axis against concentration on the x-axis. Measured on 4 March 2022

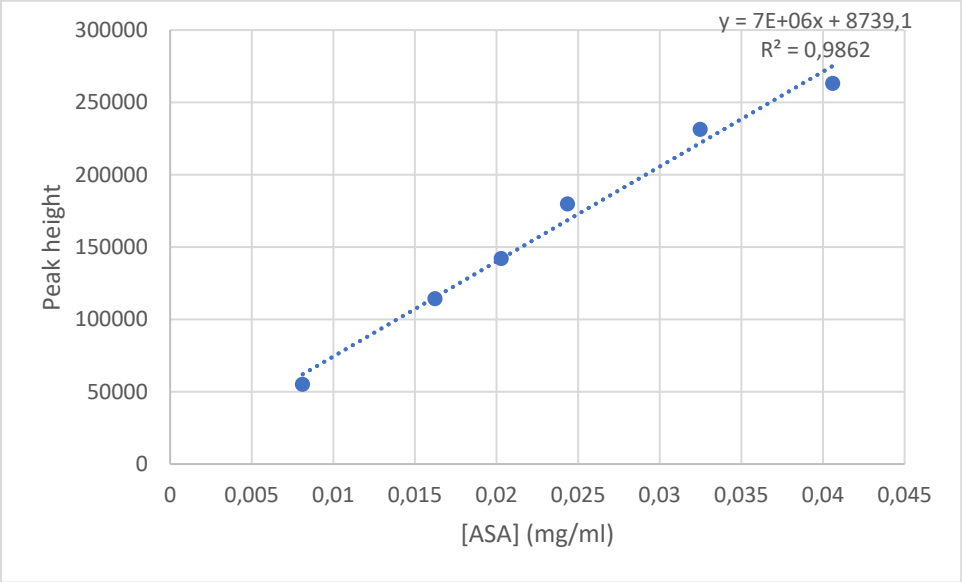

Figure S13: Calibration curve for ASA with peak height on the y-axis against concentration on the x-axis. Measured on 4 March 2022

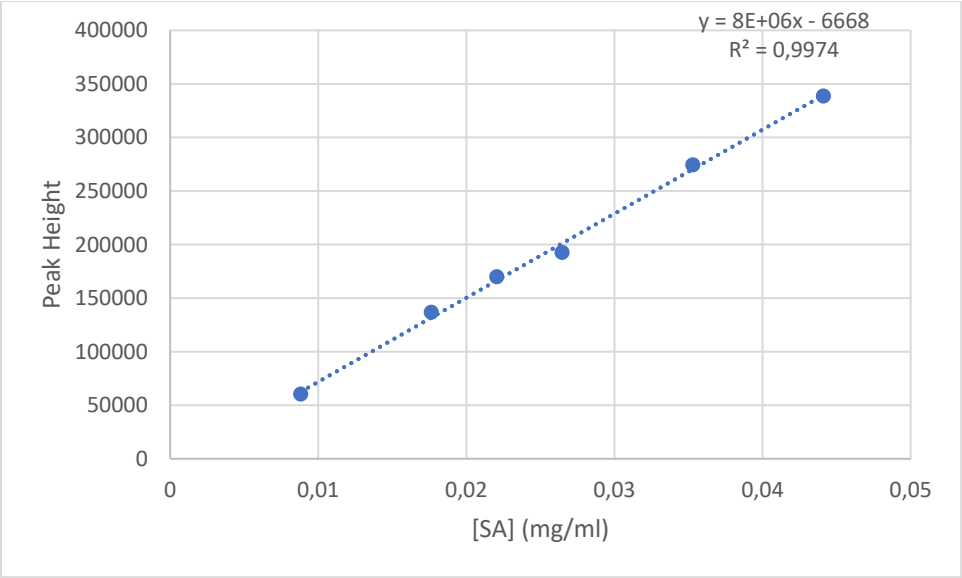

Figure S14: Calibration curve for SA with peak height on the y-axis against concentration on the x-axis. Measured on 8 March 2022

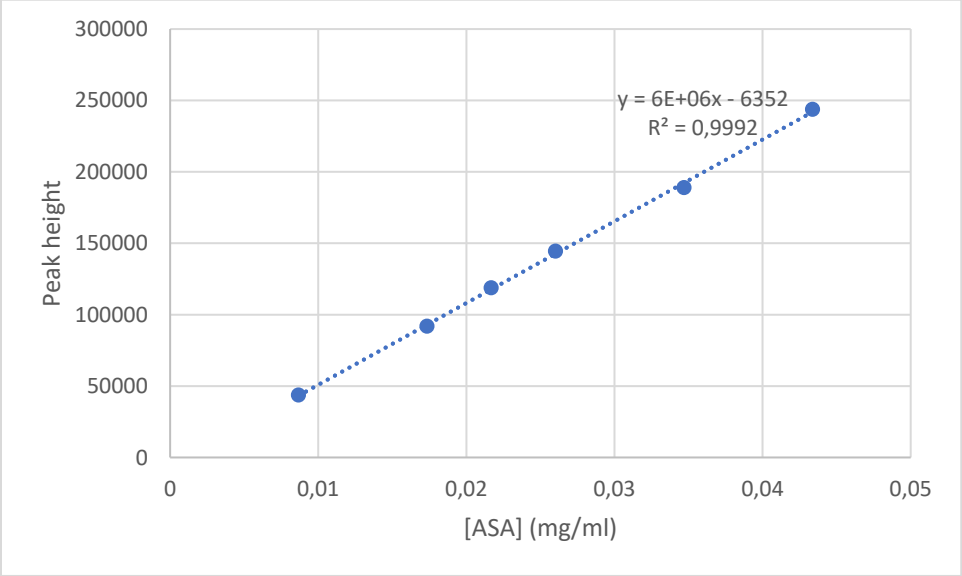

Figure S15: Calibration curve for ASA with peak height on the y-axis against concentration on the x-axis. Measured on 8 March 2022

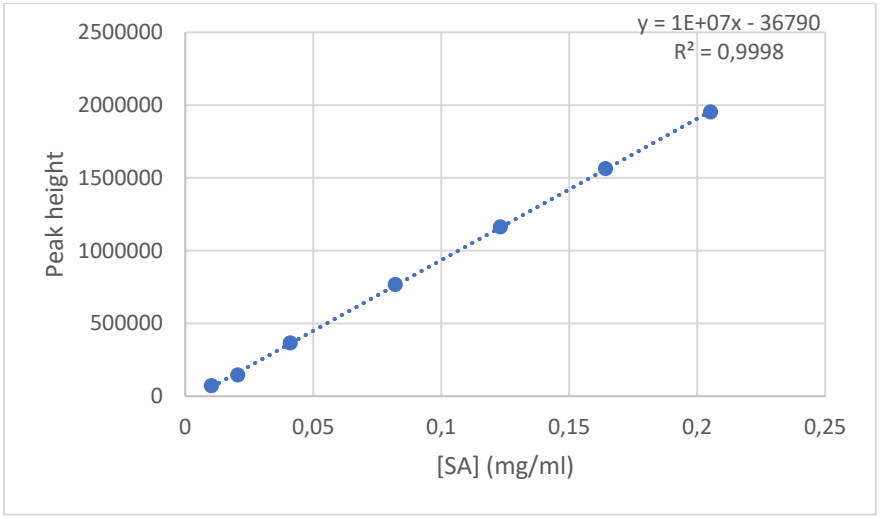

Figure S16: Calibration curve for SA with peak height on the y-axis against concentration on the x-axis. Measured on 11 March 2022

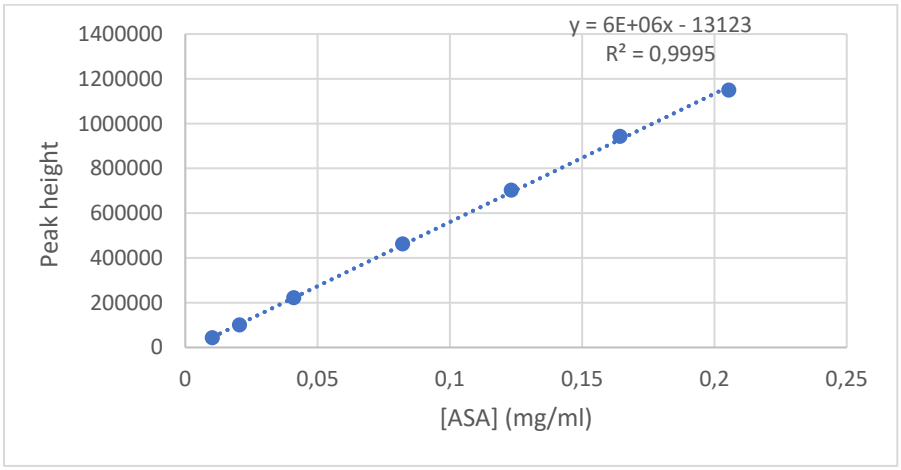

Figure S17: Calibration curve for ASA with peak height on the y-axis against concentration on the x-axis. Measured on 11 March 2022

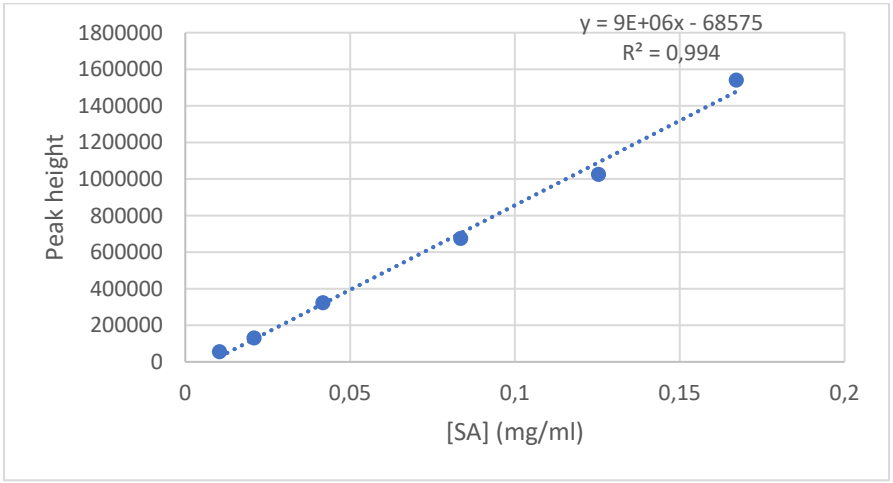

Figure S18: Calibration curve for SA with peak height on the y-axis against concentration on the x-axis. Measured on 14 March 2022

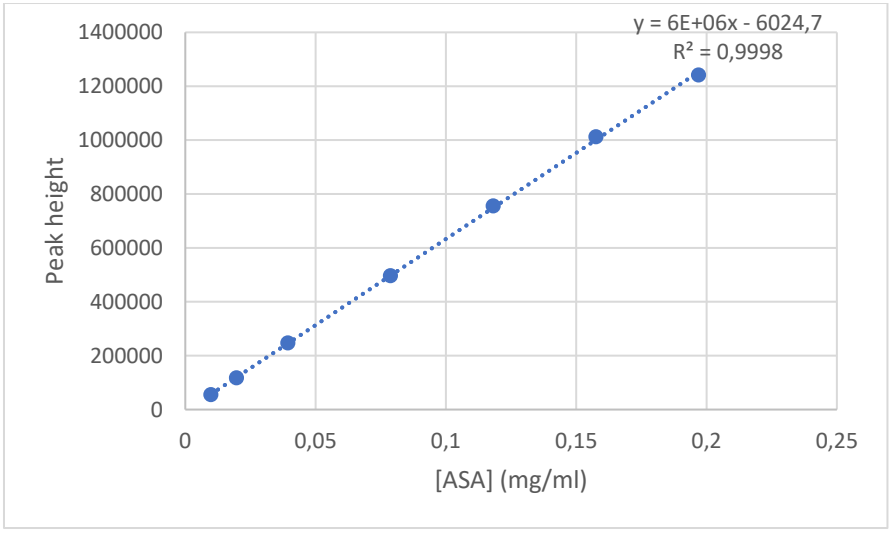

Figure S19: Calibration curve for ASA with peak height on the y-axis against concentration on the x-axis. Measured on 14 March 2022

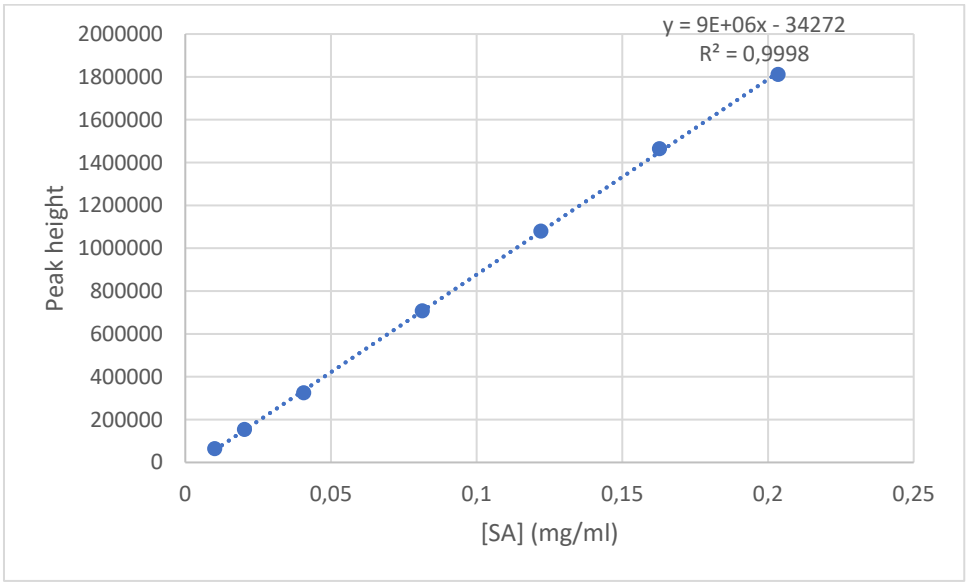

Figure S20: Calibration curve for SA with peak height on the y-axis against concentration on the x-axis. Measured on 22 March 2022

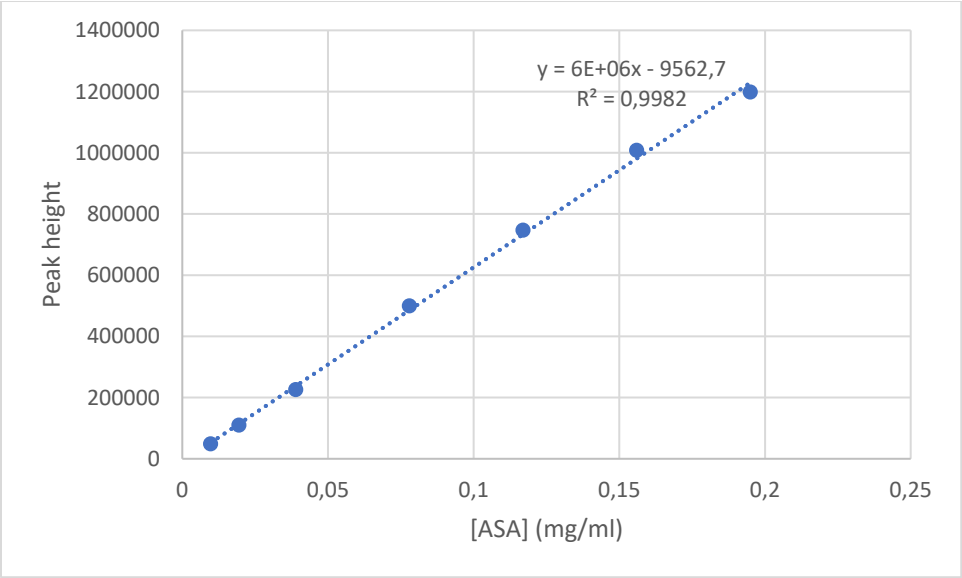

Figure S21: Calibration curve for ASA with peak height on the y-axis against concentration on the x-axis. Measured on 22 March 2022

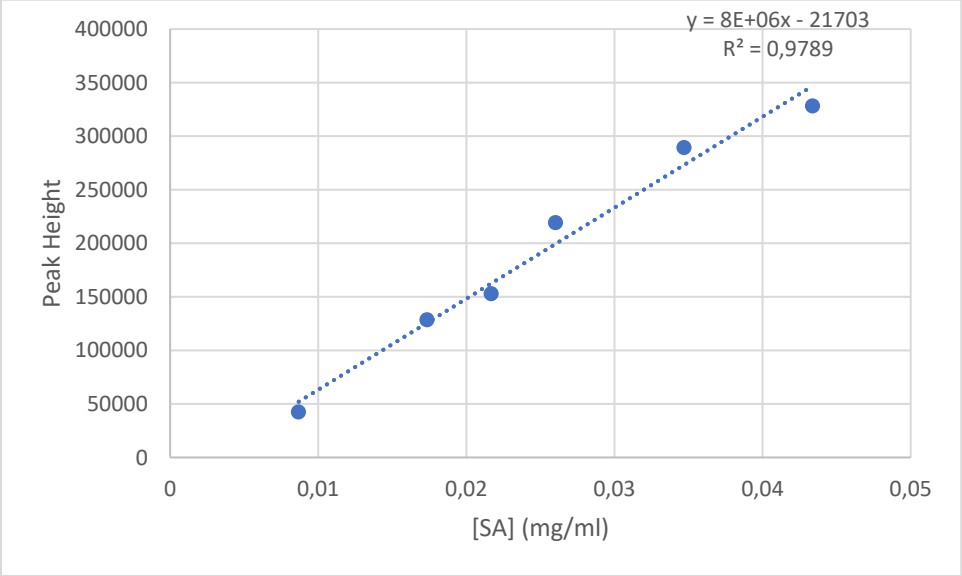

Figure S23: Calibration curve for SA with peak height on the y-axis and concentration on the x-axis. Measured on 10 March 2022

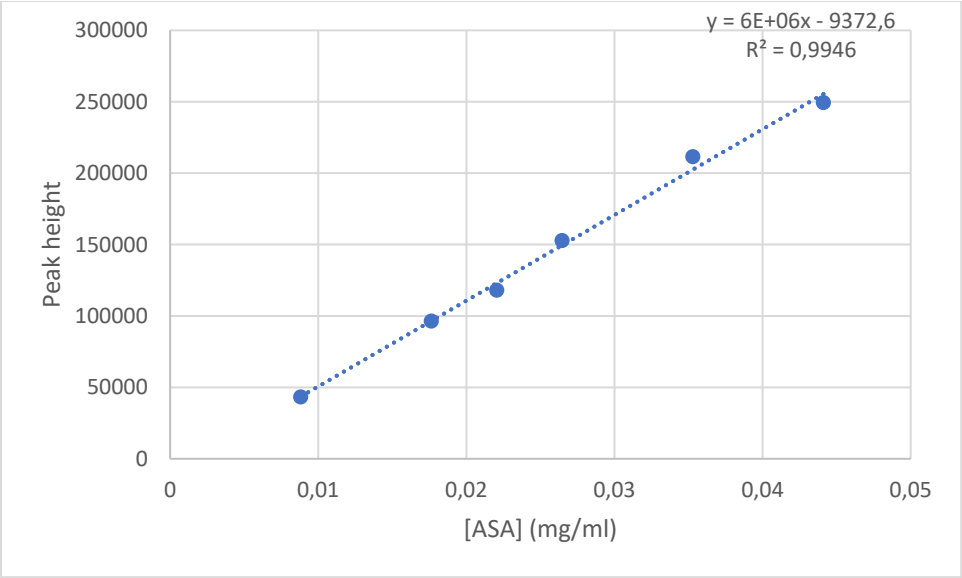

Figure S24: Calibration curve for ASA with peak height on the y-axis and concentration on the x-axis. Measured on 10 March 2022.

Appendix 4.2: Other curves

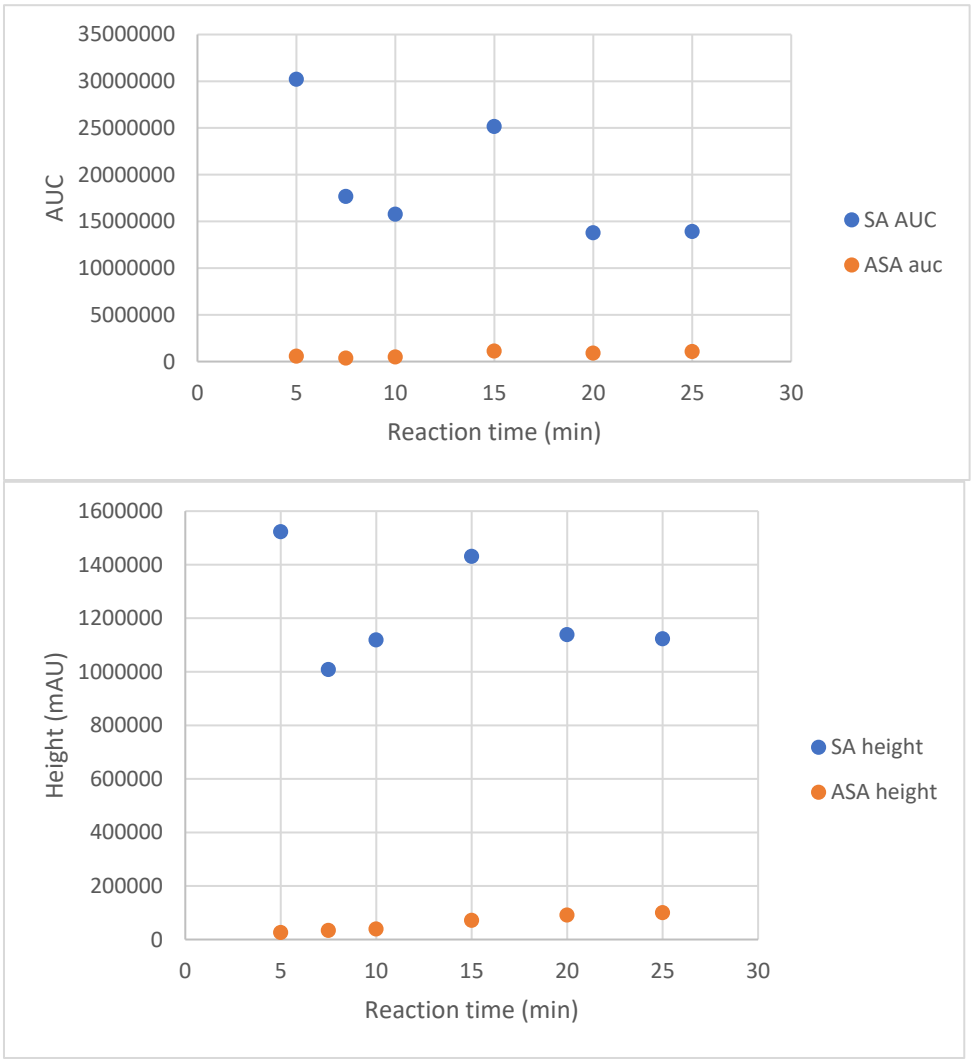

Figure S25: Data measured for prototype 2 demonstrating inconsistent AUC values and peak heights. Upper: SA and ASA AUC values measured for reaction times between 5 and 25 min. Lower: SA and ASA peak heights measured for reaction times between 5 and 25 min.

Reaction mix compound chromatograms

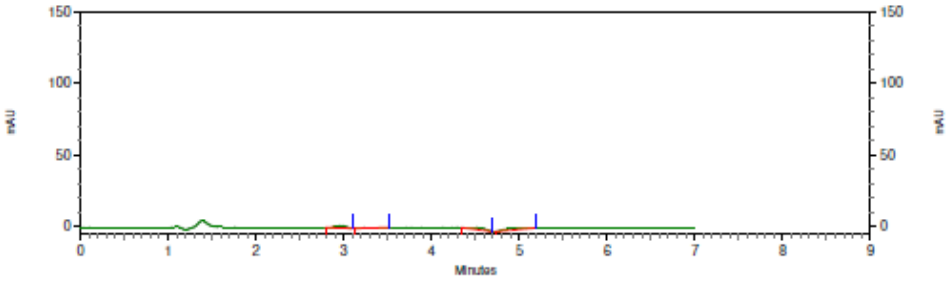

DAD-CH1 237 nm Results

Retention Time	Area	Height
2.973	50399	6896
3.360	21347	1120
4.467	70417	4258
5.147	80903	1139
Totals	223066	13413

Figure S26: Chromatogram of ethyl acetate in ACN with elution peak at 2.9 min. Measured 8 March 2022

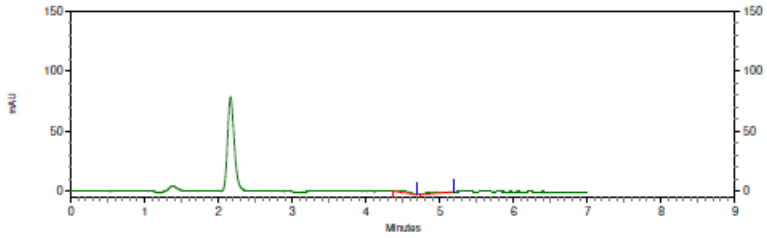

DAD-CH1 237 nm Results

Retention Time	Area	Height
4.460	55515	3182
5.153	81137	865
Totals	136652	4047

Figure S27: Chromatogram of acetic anhydride in ACN with elution peak at 2.2 min. Measured 8 March 2022

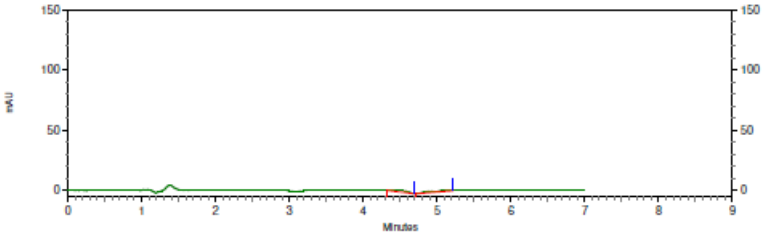

DAD-CH1 237 nm Results

Retention Time	Area	Height
4.487	68528	4863
5.167	87865	1167
Totals	156393	6030

Figure S28: Chromatogram of phosphoric acid in ACN with no visible elution peak. Measured 8 March 2022

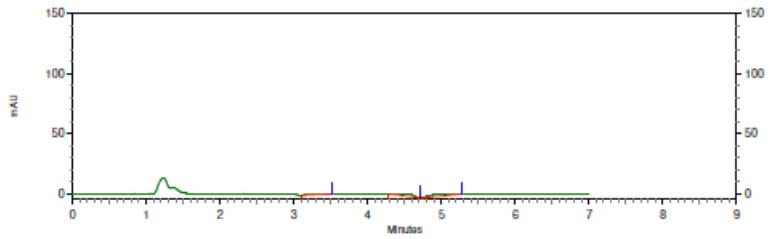

DAD-CH1 237 nm Results

Retention Time	Area	Height
3.347	39798	2137
4.487	107876	6622
5.167	128063	2748
Totals	275737	11507

Figure S29: Chromatogram of acetic acid in ACN with elution peak at 1.3 min. Measured 10 March 2022

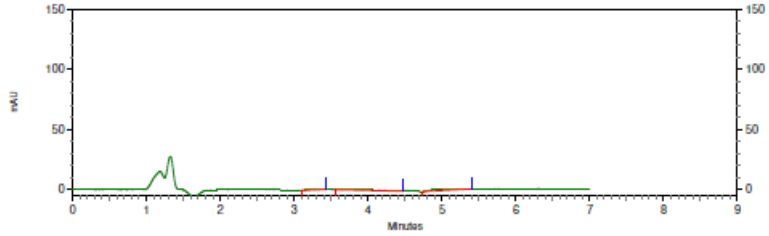

DAD-CH1 237 nm Results

Retention Time	Area	Height
3.227	28403	2842
3.607	58099	406
5.360	102845	671
Totals	189347	3919

Figure S30: Chromatogram of pure ethanol with characteristic overlapping elution leaks at 1.2 and 1.4 min. Measured 10 March 2022

Appendix 4.3: Table on where to find the raw data

Filename	Used for
22-3-2 SA c0.008	Figure S11
22-3-2 SA c0.016	Figure S11
22-3-2 SA c0.020	Figure S11
22-3-2 SA c0.024	Figure S11
22-3-2 SA c0.032	Figure S11
22-3-2 SA c0.04	Figure S11
22-3-2 ASA c0.008	Figure S12
22-3-2 ASA c0.016	Figure S12
22-3-2 ASA c0.020	Figure S12
22-3-2 ASA c0.024	Figure S12
22-3-2 ASA c0.032	Figure S12
22-3-2 ASA c0.04	Figure S12
22-3-2 5min ACN	Figure 22, 24, S25
22-3-2 7.5min ACN	Figure 22, 24, S25
22-3-2 10min ACN	Figure 22, 24, S25
22-3-2 15min ACN	Figure 22, 24, S25
22-3-2 20min ACN	Figure 22, 24, S25
22-3-2 25min ACN	Figure 22, 24, S25
22-3-2 5min EtOH	Figure 23, 24, S25
22-3-2 7.5min EtOH	Figure 23, 24, S25
22-3-2 10min EtOH	Figure 23, 24, S25
22-3-2 15min EtOH	Figure 23, 24, S25
22-3-2 20min EtOH	Figure 23, 24, S25
22-3-2 25min EtOH	Figure 23, 24, S25
22-3-4 SA c0.008	Figure S13
22-3-4 SA c0.016	Figure S13
22-3-4 SA c0.020	Figure S13
22-3-4 SA c0.024	Figure S13
22-3-4 SA c0.032	Figure S13
22-3-4 SA c0.04	Figure S13
22-3-4 ASA c0.008	Figure S14
22-3-4 ASA c0.016	Figure S14
22-3-4 ASA c0.020	Figure S14
22-3-4 ASA c0.024	Figure S14
22-3-4 ASA c0.032	Figure S14
22-3-4 ASA c0.04	Figure S14
22-3-4 20min in ACN	Figure 27, 28
22-3-4 25min in ACN	Figure 27, 28
22-3-4 30min in ACN	Figure 27, 28
22-3-4 40min in ACN	Figure 27, 28
22-3-8 SA c0.008	Figure S15
22-3-8 SA c0.016	Figure S15
22-3-8 SA c0.020	Figure S15
22-3-8 SA c0.024	Figure S15
22-3-8 SA c0.032	Figure S15
22-3-8 SA c0.04	Figure S15
22-3-8 ASA c0.008	Figure S16
22-3-8 ASA c0.016	Figure S16

22-3-8 ASA c0.020	Figure S16
22-3-8 ASA c0.024	Figure S16
22-3-8 ASA c0.032	Figure S16
22-3-8 ASA c0.04	Figure S16
22-3-8 50min in ACN	Figure 28
22-3-8 60min in ACN	Figure 28
22-3-8 90min in ACN	Figure 28
22-3-10 SA c0.008	Figure S23
22-3-10 SA c0.016	Figure S23
22-3-10 SA c0.020	Figure S23
22-3-10 SA c0.024	Figure S23
22-3-10 SA c0.032	Figure S23
22-3-10 SA c0.04	Figure S23
22-3-10 ASA c0.008	Figure S24
22-3-10 ASA c0.016	Figure S24
22-3-10 ASA c0.020	Figure S24
22-3-10 ASA c0.024	Figure S24
22-3-10 ASA c0.032	Figure S24
22-3-10 ASA c0.04	Figure S24
22-03-10 120min in ACN	Figure 28
22-03-10 180min in ACN	Figure 28
22-03-11 SA c0.01	Figure S17
22-03-11 SA c0.02	Figure S17
22-03-11 SA c0.04	Figure S17
22-03-11 SA c0.08	Figure S17
22-03-11 SA c0.12	Figure S17
22-03-11 SA c0.16	Figure S17
22-03-11 SA c0.2	Figure S17
22-03-11 ASA c0.01	Figure S18
22-03-11 ASA c0.02	Figure S18
22-03-11 ASA c0.04	Figure S18
22-03-11 ASA c0.08	Figure S18
22-03-11 ASA c0.12	Figure S18
22-03-11 ASA c0.16	Figure S18
22-03-11 ASA c0.2	Figure S18
22-03-11 180+0 in ACN	Figure 31
22-03-11 180+15 in ACN	Figure 31
22-03-11 180+30 in ACN	Figure 31
22-03-11 180+45 in ACN	Figure 31
22-03-11 180+60 in ACN	Figure 31
22-03-14 SA c0.01	Figure S19
22-03-14 SA c0.02	Figure S19
22-03-14 SA c0.04	Figure S19
22-03-14 SA c0.08	Figure S19
22-03-14 SA c0.12	Figure S19
22-03-14 SA c0.16	Figure S19
22-03-14 SA c0.2	Figure S19
22-03-14 ASA c0.01	Figure S20
22-03-14 ASA c0.02	Figure S20
22-03-14 ASA c0.04	Figure S20

22-03-14 ASA c0.08	Figure S20
22-03-14 ASA c0.12	Figure S20
22-03-14 ASA c0.16	Figure S20
22-03-14 ASA c0.2	Figure S20
22-03-14 180+0 in ACN	Figure 32
22-03-14 180+15 in ACN	Figure 32
22-03-14 180+30 in ACN	Figure 32
22-03-14 180+45 in ACN	Figure 32
22-03-14 180+60 in ACN	Figure 32
22-03-17 SA c0.01	Figure 26
22-03-17 SA c0.02	Figure 26
22-03-17 SA c0.04	Figure 26
22-03-17 SA c0.08	Figure 26
22-03-17 SA c0.12	Figure 26
22-03-17 SA c0.16	Figure 26
22-03-17 SA c0.2	Figure 26
22-03-17 ASA c0.01	Figure 26
22-03-17 ASA c0.02	Figure 26
22-03-17 ASA c0.04	Figure 26
22-03-17 ASA c0.08	Figure 26
22-03-17 ASA c0.12	Figure 26
22-03-17 ASA c0.16	Figure 26
22-03-17 ASA c0.2	Figure 26
22-03-17 0min in ACN	Figure 36
22-03-17 30min in ACN	Figure 36
22-03-17 60min in ACN	Figure 36
22-03-17 90min in ACN	Figure 36
22-03-17 120min in ACN	Figure 36
22-03-17 150min in ACN	Figure 36
22-03-17 180min in ACN	Figure 36
22-03-22 SA c0.01	Figure S21
22-03-22 SA c0.02	Figure S21
22-03-22 SA c0.04	Figure S21
22-03-22 SA c0.08	Figure S21
22-03-22 SA c0.12	Figure S21
22-03-22 SA c0.16	Figure S21
22-03-22 SA c0.2	Figure S21
22-03-22 ASA c0.01	Figure S22
22-03-22 ASA c0.02	Figure S22
22-03-22 ASA c0.04	Figure S22
22-03-22 ASA c0.08	Figure S22
22-03-22 ASA c0.12	Figure S22
22-03-22 ASA c0.16	Figure S22
22-03-2 ASA c0.2	Figure S22